ANNALS OF GEOPHYSICS, 69, 2026; doi:10.4401/ag-9511
OPEN ACCESS

The *Obsidian Sieve*: an Excel-Based Tool for Provenance Studies

Franco Foresta Martin[*,1,2]

[(1)] Istituto Nazionale di Geofisica e Vulcanologia, Sezione di Palermo, Italy
[(2)] Laboratorio Museo di Scienze della Terra, Ustica, Palermo, Italy

Article history: received November 30, 2025; accepted February 16, 2026

Abstract

This study presents the *Obsidian Sieve*, an Excel-based tool designed to provide a simple, rapid, and flexible first-step provenance assessment for Central Mediterranean obsidians using only major and minor elements. Its development was grounded in a systematic review of provenance studies that report quantitative concentrations of major and-minor oxides/elements, including chlorine (Cl), still relatively uncommon in the literature despite its high discriminant potential.

Seven bivariate systems traditionally employed in obsidian characterization were re-evaluated through a unified statistical workflow combining Kernel Density Estimation, Mahalanobis distance, 97.5% confidence ellipses, and quantitative measures of cluster overlap. This comparative analysis demonstrates that the Na_2O vs Cl diagram provides the clearest and most stable separation among the four main Italian sources, yielding the highest Discriminant Power Index and uniquely displaying non-overlapping confidence fields. These results form the statistical basis for defining conservative Na_2O-Cl windows that underpin the *Obsidian Sieve*.

The tool assigns archaeological specimens to Monte Arci, Palmarola, Pantelleria, or Lipari with high specificity, while flagging atypical or ambiguous cases as *Unknown*, thus directing research towards further analysis with more advanced geochemical techniques. Because the *Sieve* is transparent, editable, and easily adaptable, users can extend its capabilities by incorporating additional published datasets, refining source windows, or testing alternative discriminant bivariate plots. In this way, the *Obsidian Sieve* provides not only a practical screening instrument but also a flexible framework for cumulative improvement as new analytical data become available.

Keywords: Obsidian Sieve; Central Mediterranean obsidian sources; Na_2O vs Cl bivariate plot; Provenance studies; Excel-based tool

1. Introduction

This work aims to provide archaeometry researchers engaged in the geochemical characterization of Central Mediterranean obsidians with a quick diagnostic procedure that relies exclusively on major and minor elements analyses to identify the geological sources of unknown artifacts. To this end, an Excel-based tool, the *Obsidian Sieve*, downloadable in the supplementary materials as a ready-to-use spreadsheet template, is presented here. By entering

key major-minor element values, the spreadsheet automatically assigns each artifact to its original geological source or returns the warning *'Unknown'* when further investigation is required. The identification of provenance will rely primarily on the pair of elements Cl and Na_2O which, as highlighted by previous studies, has a strong discriminating power and provides a reliable basis for distinguishing the geological sources of Central Mediterranean obsidians (Foresta Martin et al., 2019, 2020).

The obsidian sources here considered are those of the four Italian insular volcanic areas: Monte Arci in Western Sardinia; Palmarola in the Pontine Islands, Latium; Pantelleria in the Sicilian Channel, Sicily; and Lipari in the Aeolian Archipelago, Sicily. These four obsidian sources supplied raw material necessary to make cutting tools to hundreds of prehistoric settlements, for thousands of years. It was a trade network scattered not only across the Italian Peninsula and surrounding islands but also in the wide Central-Western Mediterranean area, from North Africa to the Alpine Chain, from the Spanish and French coasts to the Balkan ones, through exchanges that crossed the seas and lands (Williams-Thorpe, 1995; Freund, 2018; Tykot, 2019, 2021 and references therein), (Fig. 1).

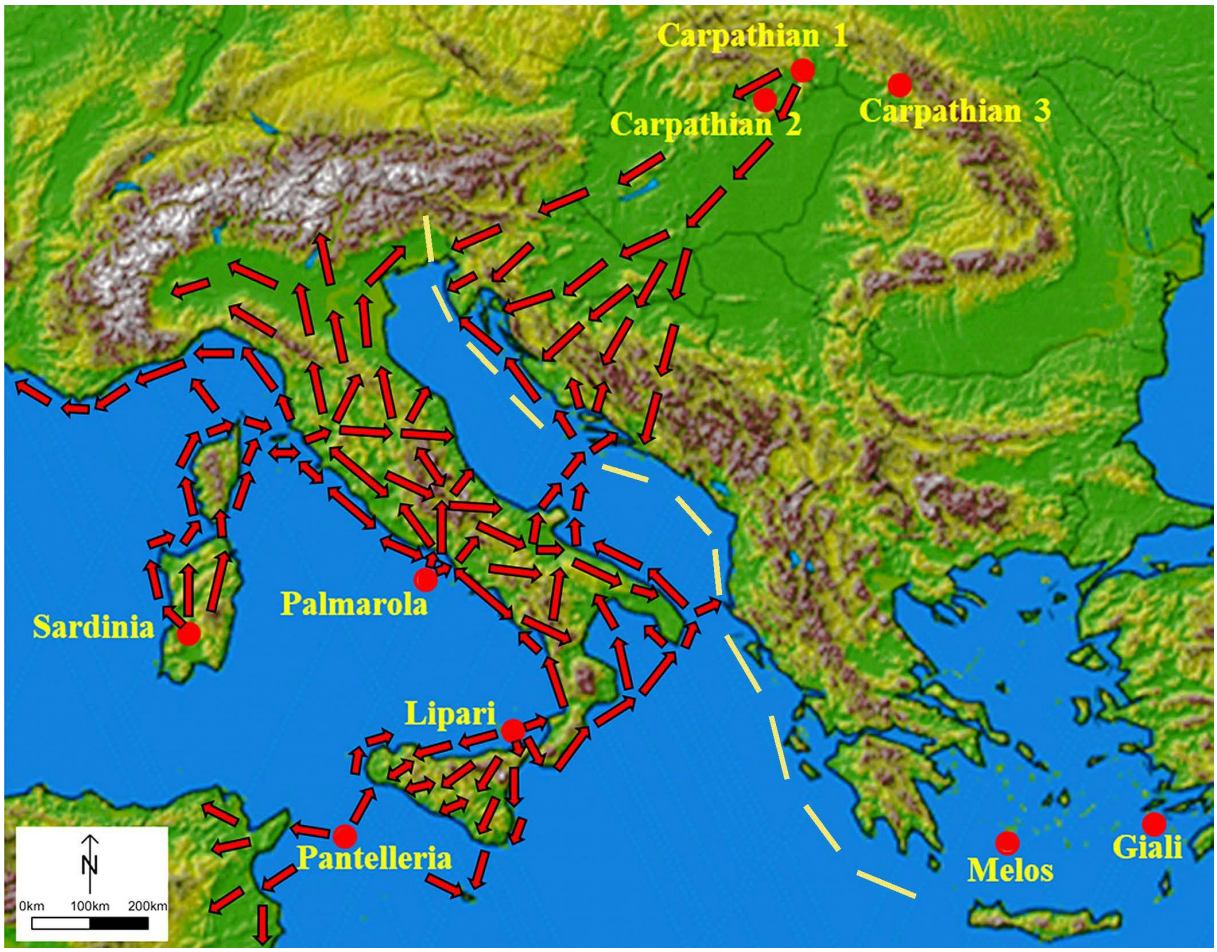

Figure 1. The Mediterranean outcrops of obsidian exploited in Prehistory can be divided into two largely independent circulation zones: Central and Eastern Mediterranean. The white dashed line materializes the Adriatic-Ionian exchange barrier, crossed only in rare and sometimes controversial cases. The red arrows reconstruct the probable distribution flows of raw material according to Tykot (2017, 2019, 2021). Modified from Tykot (2021).

Tracing the outcrops of volcanic glass from which obsidian artifacts were produced – often located far from their sites of use – makes it possible to reconstruct maritime and terrestrial exchange routes and reveal or confirm long-distance interactions between prehistoric communities (Williams-Thorpe, 1995; Freund, 2018; Tykot, 2019, 2021 and references therein). Studies on the provenance of obsidian artifacts have therefore been fundamental to understanding the trade and cultural networks developed during the long period in which obsidian tools were produced, from the Neolithic to the Bronze Age, before the introduction of metals.

Important obsidian deposits exploited in antiquity are also in the Eastern Mediterranean, on the Aegean-Greek islands of Giali and Melos; and farther east in the Carpathians, Anatolia, and Armenia (Fig. 1). Current evidence indicates that the two main Mediterranean supply zones – Central and Eastern – remained independent, with a few, exceptional exchanges documented to date along the Adriatic axis (Cann and Renfrew, 1964; Williams-Thorpe et al., 1984; Williams-Thorpe, 1995; Tykot, 1996; Carter, 2014). At Palagruža, in Croatia, within an obsidian assemblage dominated by Lipari, four artifacts from Melos were found (Forenbaher, 2018; Tykot, 2017); at Putanja, in Albania, a single Lipari artifact was recognized within a small group of Aegean pieces (Ruka et al., 2019). In the Italian Friuli-Venezia Giulia region two obsidian artifacts from the Carpathians were found: one in the Grotta della Tartaruga cave near Trieste, and another one at Sammardenchia di Pozzuolo near Udine (Williams-Thorpe et al., 1984; Tykot, 1996). A controversial case is that of the Grotta del Leone cave in Agnano, Pisa, where three small fragments were attributed to the island Melos; however, the lack of a secure stratigraphic context has led scholars to regard this attribution of doubtful value (Tykot, 1996; Ruka et al., 2019). The prevailing opinion is that all the cited cases do not reflect stable supply networks, but rather sporadic and occasional contacts, likely mediated by individual mobility or privileged personal relationships (Tykot, 2017).

In summary, more than five decades of provenance studies indicate that nearly all obsidian artifacts collected in the archaeological contexts of the large Central-Western Mediterranean area derive from the four Italian geological sources before mentioned, which constitute the focus of the present work.

2. Obsidian geochemistry

Obsidian is formed when viscous, silica-rich lavas ($SiO_2 > 70$ wt%) cool so rapidly that nucleation and crystal growth are largely inhibited. The resulting material is a volcanic glass characterized by a fully amorphous atomic structure, lacking the long-range order of a crystal lattice (Fig. 2).

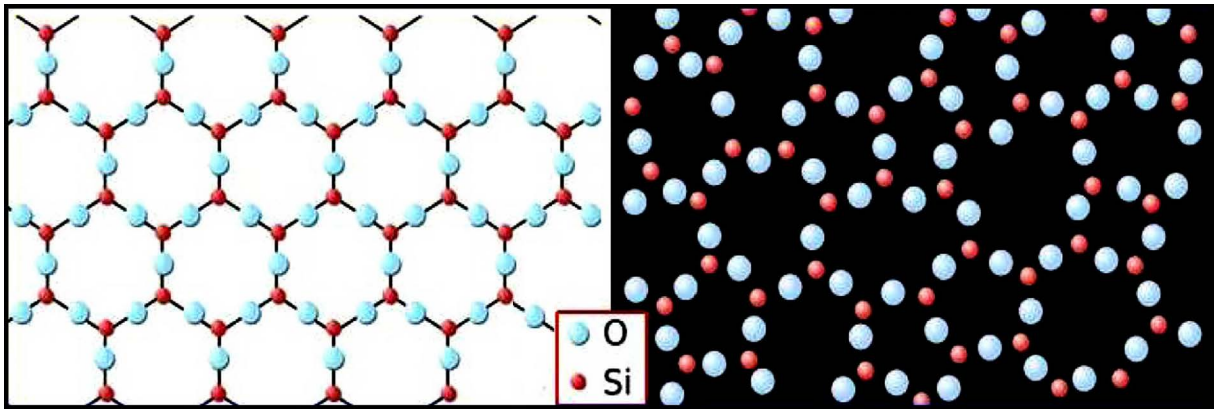

Figure 2. On the left: ordered atomic lattice of a quartz crystal (SiO_2). On the right: disordered atomic lattice of a volcanic glass of similar composition (from Foresta Martin, 2024).

In terms of bulk chemistry, the predominant concentration of SiO_2 in the obsidians is accompanied by oxides of other major elements such as Al_2O_3, Na_2O, K_2O, FeO; and minor elements such as CaO, MgO, MnO, TiO_2, Cl. Many other obsidian constituents are defined as trace elements due to their very low presence. According to the prevailing literature, the distinction between major, minor and trace elements is conventionally defined by the following thresholds (wt%): major >1, minor between 0.1-1, traces <0.1, (Rollinson and Pease, 2021).

Because major and minor elements show limited variability among the Central Mediterranean sources – with ranges often comparable to analytical uncertainty – source discrimination based solely on these oxides is generally difficult, except in cases of marked enrichment or depletion. For example, Pantelleria obsidians, derived from strongly peralkaline magmas, display the highest levels of sodium and iron contents, making them easily distinguishable from the other Central Mediterranean sources. Palmarola obsidians typically show higher sodium and lower calcium contents than Monte Arci and Lipari, although hydration or analytical bias may obscure this pattern.

Among the minor-trace elements, Cl is particularly effective at distinguishing the three geological sources of Monte Arci, Palmarola and Lipari, whose major compositions overlap. This is because Cl displays source-specific enrichments linked to magmatic differentiation and volatile behavior. Table 1 summarizes the average composition of some major and minor elements for the four Central Mediterranean obsidian sources (Monte Arci, Palmarola, Lipari, and Pantelleria), expressed as weight percentages (wt%) of their respective oxides, based on published data (see caption).

Table 1. Average composition (wt%) of some major and minor elements in the obsidians from the four Central Mediterranean sources (Monte Arci, Palmarola, Pantelleria, Lipari). The double figures for Monte Arci and Pantelleria sources refer to the average values of the respective main subgroups. Data from Acquafredda et al. (1999); De Francesco et al. (2008); Foresta Martin et al. (2017, 2020); Le Bourdonnec et al. (2010); Tykot (2002). * Some authors consider Cl as a trace element and express its content in ppm; here it has been converted to wt%.

Source	SiO_2	Al_2O_3	Na_2O	K_2O	FeOtot	CaO	Cl*
Monte Arci	73-76	13-14	3-3.5	5-5.5	1.5-2	0.6-1	0.1
Palmarola	75	13	4.5	5	1.5	0.5	0.2
Pantelleria	71-75	7-12	6-7	3.5-4.5	7.5-9	0.3-0.5	0.5
Lipari	75	13	4.00	5	1.5	0.7	0.3

Trace elements show a much wider variability between sources, making the identification of the original geological deposit more certain. Among the trace elements with high discriminatory power used for provenance studies are the alkali metals Rb and Cs, the alkaline earth metals Sr and Ba, and the transition metals Y and Zr. Table 2 reports some trace elements average composition (ppm) for the four Central Mediterranean obsidian sources, based on published data (see caption).

Table 2. Average composition (ppm) of selected trace elements of the obsidians from the four Central Mediterranean sources (Monte Arci, Palmarola, Lipari, Pantelleria). The double numerical values of Monte Arci and Pantelleria differentiate between the two main sub-sources distinguishable in each location. Data from Acquafredda et al. (1999); De Francesco et al. (2008); Tykot (2002); Foresta Martin et al. (2017).

Source	Rb	Sr	Y	Zr	Nb	Cs	Ba
Monte Arci	175-260	35-130	23-32	100-250	35-50	5	130-800
Palmarola	450	7	58-62	300	70	45	30
Pantelleria	120-180	8	107-230	1500-1900	300-400	2	50-80
Lipari	300	12	31-55	180	40	15	30

The comparison between Tables 1 and 2 clearly illustrates that while the major and minor oxides define relatively narrow and often overlapping fields for the four Central Mediterranean obsidian sources, the trace elements show much wider and largely non-overlapping ranges. This contrast explains why trace-element fingerprinting has traditionally been considered the most robust method for provenance studies (Barca et al., 2007, 2008).

According to the widely used TAS classification diagram of volcanics – Total Alkali ($Na_2O + K_2O$) vs Silica (SiO_2) – most obsidians plot within the rhyolite field, with high silica (68-76 wt%) and alkali (8-12 wt%) contents. However, depending on cooling and solidification rates, trachytes (characterized by lower silica contents compared to rhyolites)

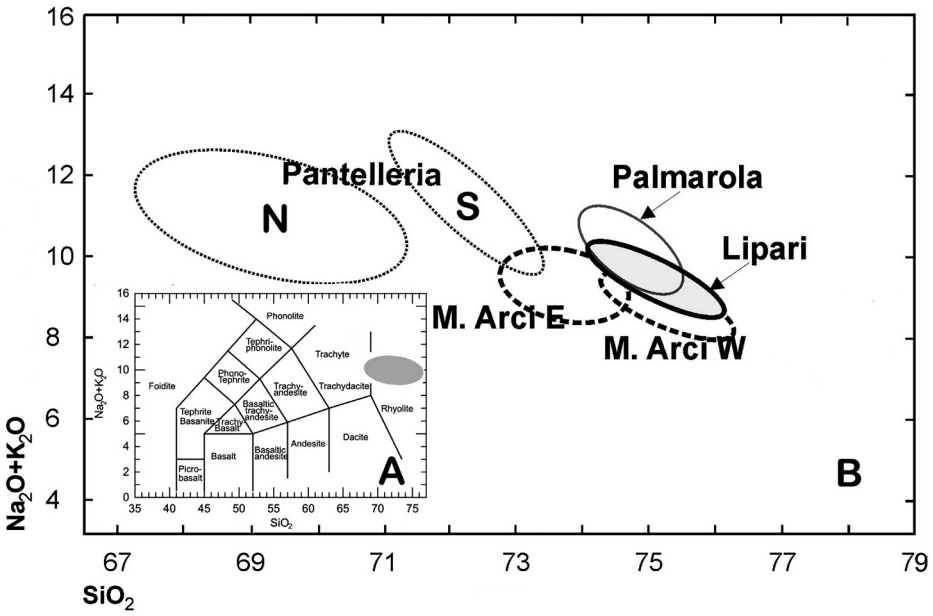

Figure 3. (A) In the classification diagram for volcanic rocks TAS (Total Alkali vs. Silica, after Le Bas, 1986) obsidians occupy mainly the rhyolite range. (B) The Tas diagram is not suitable for discriminating the four Central Mediterranean obsidian sources: except for Pantelleria, the other three sources overlap. Sometimes distinctions arise between the two sub-sources North/South of Pantelleria, and East/West of Monte Arci. (Data after Acquafredda et al., 1999; Le Bourdonnec et al., 2010; Foresta Martin et al., 2017; De Francesco et al., 2008).

can also yield obsidians: it is the case of some Pantelleria obsidians, which exhibit the lowest SiO_2 content (~67 wt%) and the highest alkali content (~12 wt%). In literature, Pantelleria obsidians with similar chemical characteristics are reported by Francaviglia (1987, 1988), Foresta Martin et al. (2017), and attributed to unspecified subsources in the north of the island. As highlighted by Rotolo et al. (2020) the location of some Pantelleria northern subsources is still controversial (Fig. 3).

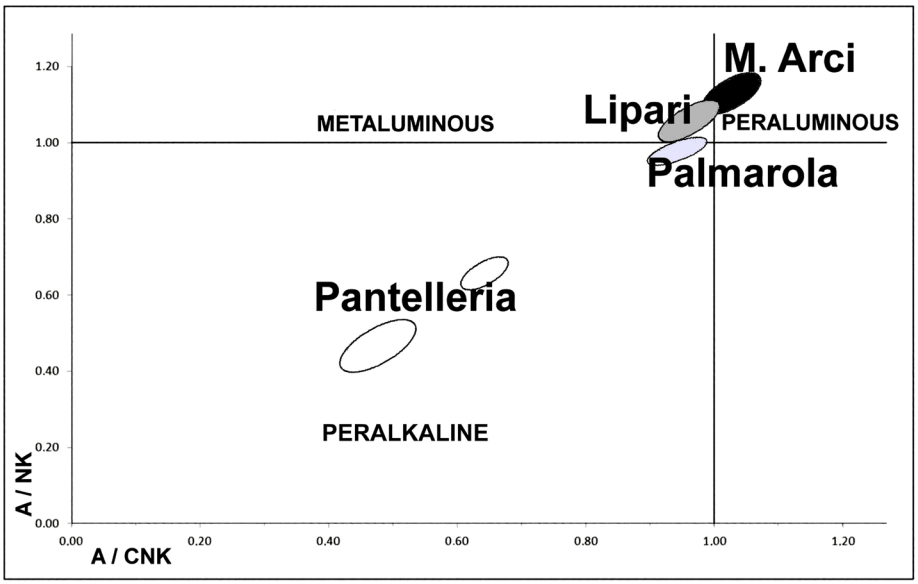

Figure 4. Shand's (1927) diagram A/CNK vs A/NK better than TAS discriminates the Central Mediterranean obsidian sources; even if it does not completely avoid overlaps between the adjacent fields of Monte Arci (peraluminous obsidians), Lipari (metaluminous) and Palmarola (peralkaline but on the border with metaluminous). Data as in Fig. 3.

Obsidian compositions can also be described using Shand's (1927) A/CNK vs A/NK diagram, where A/CNK is defined as molar $Al_2O_3/(CaO + Na_2O + K_2O)$ and A/NK as molar $Al_2O_3/(Na_2O + K_2O)$. These indices express the balance between alumina – the second most abundant oxide in igneous rocks – and the alkalis and calcium.

According to this scheme, obsidians with A/CNK > 1 are classified as peraluminous, meaning that alumina is present in relative excess. Obsidian with A/CNK < 1 but A/NK > 1 is considered metaluminous, indicating a moderate alumina deficit. Finally, peralkaline obsidians contain more alkalis than can be balanced by alumina (PI > 1.0) and are therefore also alumina-poor (A/CNK < 1) (Williams-Thorpe, 1995). Within this framework, Monte Arci obsidians fall in the peraluminous field, whereas Pantelleria obsidians in the peralkaline field (Foresta Martin et al., 2020), (Fig. 4).

2.1 Chlorine geochemical behavior in volcanic glass

The strong discriminating power of Cl for the recognition of obsidian sources is due to its incompatible behavior during magmatic differentiation, which causes it to concentrate in the residual melt rather than partitioning into crystalline phases (Foresta Martin et al., 2020 and references therein). Since the early 20th century, it has been found that some silicic volcanic glasses contain much more Cl than typical igneous rocks. Rhyolitic obsidians typically display 0.1-0.4 wt% Cl concentrations, whereas pantelleritic peralkaline glasses may reach 1.0 wt%. In contrast, most igneous rocks contain only 0.02 wt% of Cl (Lowenstern, 1994). Cl behaves as a highly incompatible component during magmatic evolution: it does not enter the structure of feldspars or ferromagnesian minerals and therefore accumulates in SiO_2-rich residual melts produced by fractional crystallization, leading to its higher contents in evolved magmas such as trachytes and rhyolites (Bonifacie et al., 2008).

Experimental studies furthermore show that Cl solubility rises in melts enriched in network-modifying cations (Na, K, Mg, Ca, Fe), which increase the NBO/T (Non-Bridging Oxygen per Tetrahedron) and facilitate incorporation of Cl into the melt structure. Thus, peralkaline rhyolitic melts display the highest Cl solubilities owing to their low degree of polymerization and high activities of Na^+ and K^+, reaching the highest values in peralkaline systems (Métrich and Rutherford, 1992; Carroll and Webster, 1994; Carroll, 2005). For these reasons, the joint use of Na_2O and Cl provides a robust and mutually reinforcing discrimination of the four Central Mediterranean obsidian sources (Foresta Martin et al., 2019, 2020).

2.2 Analytics for obsidian geochemical characterization

A wide range of analytical techniques is available for the geochemical characterization of the obsidian findings in a non-destructive or minimally destructive manner. Among the most frequently employed are scanning electron microscopy (SEM), electron probe microanalysis (EPMA), X-ray fluorescence (XRF), and laser ablation inductively coupled plasma mass spectrometry (LA-ICP-MS). These techniques enable the measurement of major, minor, and trace elements, thereby providing the geochemical fingerprint of an obsidian archaeological artifact and linking it to its geological source.

A consolidated protocol developed in recent decades usually involves two successive analytical steps: 1) determination of major and minor element concentrations; 2) trace element characterization. In this way, a comprehensive geochemical profile of the artifacts is obtained, supporting a robust provenance attribution (Acquafredda et al., 1999; De Francesco et al., 2008; Tykot, 2002; Foresta Martin et al., 2017).

Another effective geochemical approach that can be employed for determining the provenance of obsidian consists in the measurement of radiogenic isotope ratios such as $^{87}Sr/^{86}Sr$ and $^{143}Nd/^{144}Nd$. These isotopic systems record the long-term geochemical evolution of the magmatic sources from which each obsidian derives and are only minimally affected by secondary alteration processes. As a result, even closely related volcanic districts often display distinct isotopic fingerprints that can be used to trace the origin of archaeological specimens (e.g., Cariddi et al., 2026, and references therein). Although such isotopic analyses represent a highly discriminant tool for sourcing obsidian, they are generally more demanding – both in terms of analytical time and operational costs – than the geochemical techniques most employed in provenance studies (e.g., SEM-EDS, XRF, LA-ICP-MS).

Since researchers working on obsidian provenance aim to achieve reliable geochemical characterizations with minimal financial and time investment, the present study proposes an approach that requires the acquisition of discriminant major/minor elements through the most accessible and expeditious analytical tools. Entrusted to

the *Obsidian Sieve*, these data will allow the attribution of obsidian samples to their respective geological sources, evidencing those considered *Unknown*. In this way, the most expensive and time-consuming analytical methods can be limited to finds of uncertain origin.

3. Assembling the obsidian analysis dataset

The analytical data used in this study were compiled from published works reporting major, minor, and trace element analyses of geological and archaeological obsidian samples, including Cl. Because the *Obsidian Sieve* relies on Na_2O and Cl as its discriminant variables, only studies providing Cl measurements were included. Unfortunately, only a limited number of papers report Cl concentrations of Mediterranean obsidians (Francaviglia, 1984, 1987, 1988, 1999; MacDonald and Smith, 1992; Tykot, 2002; Foresta Martin et al., 2019, 2020; Kasztovszky et al., 2019), and even fewer explicitly propose Cl as a discriminant parameter for provenance analysis (Foresta Martin et al., 2019, 2020).

Geological obsidians included in the database were sampled by the cited authors from the four Central Mediterranean sources: Monte Arci, Palmarola, Pantelleria, and Lipari. Archaeological samples were assigned by the same authors to their original sources, based on major-minor and trace-element fingerprints. The resulting dataset comprises 262 entries: 71 geological and 191 archaeological samples (Table 3).

Table 3. Number of geological and archaeological entries contained in the dataset of chemical analyses of Monte Arci, Palmarola, Pantelleria, and Lipari obsidian sources.

Source	Geological	Archaeological	Total
Monte Arci	32	5	37
Palmarola	7	2	9
Pantelleria	19	26	45
Lipari	13	158	171
All Sources	71	191	262

For each item, the dataset reports the wt% concentrations of the following oxides/elements: SiO_2, TiO_2, Al_2O_3, FeOtot, MnO, MgO, CaO, Na_2O, K_2O, P_2O_5, and Cl; the sum of their wt% concentrations has a median value of 99.7%.

To ensure comparability across studies, two standardizations were applied. (i) Cl values originally reported in ppm were converted to wt% (wt% = ppm/10,000), since Cl is treated here as a minor element. (ii) When iron was reported as Fe_2O_3, it was converted to FeOtot (FeOtot = $Fe_2O_3 \times 0.8998$).

For several geological samples, some authors reported averaged values obtained from multiple fragments collected at the same outcrop locality (e.g., Francaviglia, 1984, 1999; Tykot, 2002). Consequently, part of the dataset consists of 'virtual samples', whose compositions represent the mean chemistry of a specific outcrop sector rather than a single hand specimen. For archaeological specimens, it is reasonable to assume that provenance assignments reported in the literature are reliable, being based on trace-element analyses performed by the original authors.

Despite the heterogeneity of sampling strategies and analytical procedures adopted by different authors, the assembled database represents the geochemical signatures of the four Central Mediterranean obsidian outcrops. Its diversity makes it a rigorous testbed for evaluating the effectiveness of provenance procedures based exclusively on major and minor elements.

Table 4 a,b,c,d specifies, for each of the 262 entries: source, type (geological/archaeological), sampling location details, bibliographic reference of the paper from which the data are taken, and chemical analyses of major/minor elements.

Table 4/a, b, c, d. Database of 262 entries (71 geological and 191 archaeological) of major/minor obsidians chemical analyses, taken from literature. a) Monte Arci; b) Palmarola; c) Pantelleria; d) Lipari. Locations, authors and bibliographic references, in the first column. Totals slightly above 100% reflect analytical uncertainties and rounding.

Table 4/a. Monte Arci.

No.	Source, Type, Location, Author	SiO_2	TiO_2	Al_2O_3	FeOtot	MnO	MgO	CaO	Na_2O	K_2O	P_2O_5	Cl	Tot%
1	MONTE ARCI, GEO, SA, Conca 'e Cannas (Foresta Martin et al., 2020)	75.54	0.07	13.26	1.13	0.06	0.08	0.55	3.42	5.48	0.11	0.13	99.83
2	MONTE ARCI, GEO, SA, Conca 'e Cannas (Foresta Martin et al., 2020)	75.89	0.10	13.11	1.04	0.05	0.06	0.51	3.41	5.45	0.08	0.14	99.84
3	MONTE ARCI, GEO, SA, Conca 'e Cannas (Foresta Martin et al., 2020)	75.38	0.11	13.41	1.12	0.06	0.08	0.58	3.48	5.38	0.08	0.13	99.81
4	MONTE ARCI, GEO, SB1, M. Sparau (Foresta Martin et al., 2020)	74.43	0.18	13.82	1.05	0.02	0.05	0.71	3.42	5.95	0.11	0.10	99.84
5	MONTE ARCI, GEO, SB1, M. Sparau (Foresta Martin et al., 2020)	74.56	0.21	13.72	0.97	0.04	0.07	0.70	3.42	5.96	0.12	0.11	99.88
6	MONTE ARCI, GEO, SB1, M. Sparau (Foresta Martin et al., 2020)	74.53	0.17	13.76	1.02	0.03	0.09	0.71	3.41	5.88	0.12	0.10	99.82
7	MONTE ARCI, GEO, SB2, Conca 'e Ollastu (Foresta Martin et al., 2020)	74.29	0.22	13.75	1.00	0.03	0.12	0.73	3.62	5.94	0.10	0.09	99.89
8	MONTE ARCI, GEO, SB2, Conca 'e Ollastu (Foresta Martin et al., 2020)	74.38	0.21	13.84	0.85	0.03	0.08	0.72	3.56	6.00	0.11	0.09	99.87
9	MONTE ARCI, GEO, SB2, Conca 'e Ollastu (Foresta Martin et al., 2020)	74.51	0.22	13.77	0.91	0.03	0.12	0.70	3.72	5.70	0.09	0.09	99.86
10	MONTE ARCI, GEO, SC, Acqua Frida (Foresta Martin et al., 2020)	73.58	0.30	13.99	1.26	0.04	0.18	0.83	3.26	6.18	0.14	0.08	99.84
11	MONTE ARCI, GEO, SC, Acqua Frida (Foresta Martin et al., 2020)	73.94	0.25	13.86	1.16	0.03	0.14	0.83	3.25	6.18	0.13	0.08	99.85
12	MONTE ARCI, GEO, SC, Acqua Frida (Foresta Martin et al., 2020)	74.22	0.27	13.75	0.90	0.03	0.07	0.72	3.23	6.48	0.10	0.09	99.86
13	MONTE ARCI, GEO, (Kasztovszky et al., 2019)	75.10	0.18	12.80	1.52	0.05	–	0.70	3.80	5.53	0.00	0.10	99.78
14	MONTE ARCI, GEO, (MacDonald et al., 1992)	74.30	0.26	13.86	1.60	0.07	0.21	0.70	3.50	5.05	0.07	0.12	99.74
15	MONTE ARCI, GEO, SA, (Tykot, 2002)	74.72	0.09	13.40	1.25	0.08	0.08	0.59	3.44	5.26	0.06	0.09	99.06
16	MONTE ARCI, GEO, SB1, (Tykot, 2002)	73.77	0.18	13.68	1.31	0.11	0.13	0.75	3.34	5.63	0.04	0.06	99.00
17	MONTE ARCI, GEO, SB1, (Tykot, 2002)	74.01	0.15	13.61	1.33	0.09	0.11	0.74	3.39	5.49	0.05	0.07	99.04
18	MONTE ARCI, GEO, SB1, (Tykot,, 2002)	74.14	0.16	13.56	1.21	0.09	0.10	0.74	3.43	5.48	0.04	0.05	99.00
19	MONTE ARCI, GEO, SB2, (Tykot, 2002)	75.05	0.13	12.97	1.17	0.08	0.11	0.57	3.34	5.51	0.04	0.07	99.04
20	MONTE ARCI, GEO, SC1, (Tykot, 2002)	72.48	0.28	14.03	1.57	0.13	0.25	0.88	3.28	5.96	0.03	0.05	98.94
21	MONTE ARCI, GEO, SC2, (Tykot, 2002)	72.68	0.26	14.01	1.47	0.14	0.18	0.87	3.30	5.94	0.03	0.05	98.93

No.	Source, Type, Location, Author	SiO_2	TiO_2	Al_2O_3	FeOtot	MnO	MgO	CaO	Na_2O	K_2O	P_2O_5	Cl	Tot%
22	MONTE ARCI, GEO, Uras, (Francaviglia, 1999)	74.61	0.12	13.29	1.46	0.07	0.03	0.54	3.61	5.48	0.03	0.02	99.26
23	MONTE ARCI, GEO, Marrubiu,(Francaviglia, 1999)	74.65	0.18	13.03	1.56	0.05	0.08	0.59	3.52	5.66	0.03	0.02	99.37
24	MONTE ARCI, GEO, Pinna, (Francaviglia, 1999)	72.81	0.34	13.78	1.91	0.04	0.16	0.83	3.45	6.12	0.05	0.01	99.50
25	MONTE ARCI, GEO, Ceca A (Francaviglia, 1999)	73.32	0.23	13.39	1.67	0.04	0.10	0.61	3.77	5.56	0.03	0.02	98.74
26	MONTE ARCI, GEO, Ceca B (Francaviglia, 1999)	75.12	0.11	12.19	1.48	0.06	0.01	0.40	4.56	4.79	0.01	0.03	98.76
27	MONTE ARCI, GEO, Pau, (Francaviglia, 1984)	72.48	0.32	14.37	1.79	0.04	0.37	0.93	3.31	5.56	0.10	0.06	99.33
28	MONTE ARCI, GEO, Marrubiu, (Francaviglia, 1984)	73.98	0.17	13.71	1.54	0.06	0.26	0.71	3.63	5.24	0.10	0.08	99.48
29	MONTE ARCI, GEO, Uras, (Francaviglia, 1984)	74.30	0.09	13.83	1.39	0.07	0.17	0.58	3.70	4.97	0.07	0.09	99.26
30	MONTE ARCI, GEO, Pinna, (Francaviglia, 1984)	72.40	0.32	14.34	1.76	0.08	0.32	0.94	3.58	5.65	0.11	0.06	99.56
31	MONTE ARCI, GEO, Ceca1, (Francaviglia, 1984)	75.00	0.09	12.68	1.43	0.07	0.13	0.44	4.29	4.57	0.02	0.17	98.89
32	MONTE ARCI, GEO, Ceca2, (Francaviglia, 1984)	72.69	0.23	14.07	1.65	0.06	0.30	0.74	3.74	5.39	0.08	0.08	99.03
33	MONTE ARCI, ARCH, 3, Puisteris (Francaviglia, 1984)	71.94	0.34	14.62	2.12	0.04	0.35	0.91	3.42	5.31	0.08	0.06	99.19
34	MONTE ARCI, ARCH, 4, Puisteris (Francaviglia, 1984)	74.19	0.11	13.95	1.68	0.06	0.17	0.59	3.56	4.81	0.05	0.09	99.26
35	MONTE ARCI, ARCH, 5, Losa (Francaviglia, 1984)	71.95	0.37	13.34	2.03	0.04	0.39	1.11	3.36	5.58	0.08	0.06	98.31
36	MONTE ARCI, ARCH, 6, Losa (Francaviglia, 1984)	74.62	0.22	11.51	2.48	0.13	0.13	0.15	5.15	4.13	0.02	0.13	98.67
37	MONTE ARCI, ARCH, 7, Omodeo (Francaviglia, 1984)	72.10	0.35	14.23	2.10	0.04	0.29	0.95	3.29	5.56	0.08	0.06	99.05

Table 4/b. Palmarola.

No.	Source, Type, Location, Author	SiO_2	TiO_2	Al_2O_3	FeOtot	MnO	MgO	CaO	Na_2O	K_2O	P_2O_5	Cl	Tot%
38	PALMAROLA, GEO, CDF, (Foresta Martin et al., 2020)	75.18	0.10	13.05	0.96	0.06	0.01	0.24	4.81	5.16	0.02	0.22	99.81
39	PALMAROLA, GEO, CDF., (Foresta Martin et al., 2020)	75.05	0.11	13.12	0.97	0.07	0.01	0.23	4.81	5.22	0.02	0.21	99.82
40	PALMAROLA, GEO, CDF., (Foresta Martin et al., 2020)	75.03	0.07	13.05	1.06	0.08	0.03	0.31	4.73	5.21	0.03	0.22	99.82
41	PALMAROLA, GEO, RAD., (Foresta Martin et al., 2020)	74.96	0.09	13.04	1.10	0.05	0.02	0.26	4.78	5.24	0.02	0.22	99.78

No.	Source, Type, Location, Author	SiO_2	TiO_2	Al_2O_3	FeOtot	MnO	MgO	CaO	Na_2O	K_2O	P_2O_5	Cl	Tot%
42	PALMAROLA, GEO, RAD., (Foresta Martin et al., 2020)	74.54	0.10	12.95	1.49	0.09	0.04	0.46	4.78	5.15	0.02	0.21	99.83
43	PALMAROLA, GEO, RAD., (Foresta Martin et al., 2020)	74.59	0.08	12.98	1.49	0.09	0.04	0.44	4.73	5.15	0.02	0.20	99.81
44	PALMAROLA, GEO, Tram., (Francaviglia, 1999)	73.63	0.11	12.75	1.82	0.09	0.01	0.44	4.94	5.18	0.01	0.04	99.02
45	PALMAROLA, ARCH, UST-49, (Foresta Martin et al., 2020)	75.86	0.05	13.56	1.28	0.09	0.08	0.32	4.75	5.17	0.04	0.22	101.42
46	PALMAROLA, ARCH, from Pontina, (Francaviglia, 1984)	73.55	0.12	13.34	2.03	0.08	0.12	0.51	4.71	4.65	0.02	0.15	99.28

Table 4/c. Pantelleria.

No.	Source, Type, Location, Author	SiO_2	TiO_2	Al_2O_3	FeOtot	MnO	MgO	CaO	Na_2O	K_2O	P_2O_5	Cl	Tot%
47	PANTELLERIA, GEO, FP1, (Foresta Martin et al., 2020)	70.45	0.50	10.61	5.73	0.29	0.21	0.36	6.32	4.86	0.05	0.36	99.74
48	PANTELLERIA, GEO, FP1, (Foresta Martin et al., 2020)	70.69	0.45	10.92	5.39	0.26	0.22	0.35	6.30	4.78	0.02	0.35	99.73
49	PANTELLERIA, GEO, BDT, (Foresta Martin et al., 2020)	72.50	0.19	7.66	6.71	0.28	0.03	0.24	7.41	4.15	0.03	0.49	99.69
50	PANTELLERIA, GEO, BDT, (Foresta Martin et al., 2020)	71.87	0.21	7.44	7.51	0.31	0.03	0.24	7.21	4.31	0.02	0.50	99.65
51	PANTELLERIA, GEO, BDT, (Foresta Martin et al., 2020)	72.20	0.21	7.46	7.06	0.29	0.03	0.24	7.34	4.22	0.03	0.49	99.57
52	PANTELLERIA, GEO, BDT, (Foresta Martin et al., 2020)	72.17	0.22	7.59	7.04	0.30	0.03	0.23	7.16	4.38	0.02	0.52	99.66
53	PANTELLERIA, GEO, BDT, (Foresta Martin et al., 2020)	72.39	0.21	7.76	6.73	0.26	0.03	0.24	7.29	4.26	0.03	0.50	99.70
54	PANTELLERIA, GEO, SLV, (Foresta Martin et al., 2020)	71.65	0.21	7.47	7.63	0.32	0.03	0.24	7.28	4.31	0.03	0.51	99.68
55	PANTELLERIA, ARCH, UST-6, (Foresta Martin et al., 2020)	71.72	0.27	7.85	7.82	0.28	0.12	0.24	7.09	4.28	0.05	0.49	100.21
56	PANTELLERIA, ARCH, UST-10, (Foresta Martin et al., 2020)	66.93	0.64	11.51	7.70	0.32	0.25	0.54	7.42	4.66	0.06	0.26	100.29
57	PANTELLERIA, ARCH, UST-18, (Foresta Martin et al., 2020)	71.38	0.20	7.74	7.60	0.36	0.07	0.27	7.11	4.59	0.03	0.50	99.85
58	PANTELLERIA, ARCH, UST-21, (Foresta Martin et al., 2020)	71.89	0.27	7.80	7.87	0.37	0.09	0.24	6.99	4.37	0.02	0.50	100.41
59	PANTELLERIA, ARCH, UST-33, (Foresta Martin et al., 2020)	71.64	0.26	7.82	7.79	0.34	0.06	0.24	7.04	4.08	0.03	0.42	99.72
60	PANTELLERIA, ARCH, UST-40, (Foresta Martin et al., 2020)	72.38	0.20	7.89	7.84	0.29	0.10	0.27	6.78	4.17	0.02	0.51	100.45
61	PANTELLERIA, ARCH, UST-48, (Foresta Martin et al., 2020)	72.86	0.23	7.96	7.66	0.34	0.10	0.19	7.04	4.48	0.05	0.51	101.42

No.	Source, Type, Location, Author	SiO_2	TiO_2	Al_2O_3	FeOtot	MnO	MgO	CaO	Na_2O	K_2O	P_2O_5	Cl	Tot%
62	PANTELLERIA, ARCH, UST-56, (Foresta Martin et al., 2020)	71.46	0.22	7.88	7.75	0.31	0.08	0.24	6.53	4.29	0.02	0.51	99.29
63	PANTELLERIA, ARCH, UST-61, (Foresta Martin et al., 2020)	71.24	0.24	7.68	7.82	0.35	0.12	0.23	6.95	4.34	0.03	0.49	99.49
64	PANTELLERIA, ARCH, UST-77, (Foresta Martin et al., 2020)	71.55	0.16	7.71	7.79	0.32	0.13	0.20	6.82	4.49	0.02	0.42	99.61
65	PANTELLERIA, ARCH, UST-78, (Foresta Martin et al., 2020)	72.21	0.19	7.64	7.81	0.29	0.12	0.23	6.83	4.18	0.02	0.43	99.95
66	PANTELLERIA, ARCH, UST-80, (Foresta Martin et al., 2020)	71.56	0.19	7.79	7.85	0.35	0.06	0.23	6.80	4.71	0.03	0.49	100.06
67	PANTELLERIA, ARCH, UST-82, (Foresta Martin et al., 2020)	71.62	0.25	7.77	7.83	0.32	0.10	0.29	6.84	4.23	0.03	0.50	99.78
68	PANTELLERIA, ARCH, UST-85, (Foresta Martin et al., 2020)	71.46	0.19	7.67	7.34	0.31	0.11	0.20	6.68	4.67	0.02	0.53	99.18
69	PANTELLERIA, ARCH, UST-96, (Foresta Martin et al., 2020)	71.91	0.21	7.27	7.94	0.34	0.12	0.24	6.74	4.37	0.02	0.56	99.72
70	PANTELLERIA, ARCH, UST-104, (Foresta Martin et al., 2020)	72.11	0.24	7.77	7.94	0.31	0.11	0.27	7.11	4.24	0.04	0.52	100.66
71	PANTELLERIA, ARCH, UST-112, (Foresta Martin et al., 2020)	71.97	0.25	7.93	7.63	0.30	0.10	0.22	6.86	4.71	0.03	0.46	100.46
72	PANTELLERIA, ARCH, UST-126, (Foresta Martin et al., 2020)	71.77	0.26	7.78	7.78	0.36	0.10	0.28	6.78	4.20	0.02	0.51	99.84
73	PANTELLERIA, ARCH, UST-137, (Foresta Martin et al., 2020)	71.30	0.22	7.80	7.64	0.29	0.11	0.26	6.61	4.31	0.02	0.52	99.08
74	PANTELLERIA, ARCH, UST-153, (Foresta Martin et al., 2020)	71.40	0.25	7.82	7.82	0.31	0.08	0.26	6.54	4.47	0.02	0.53	99.50
75	PANTELLERIA, ARCH, UST-165, (Foresta Martin et al., 2020)	70.43	0.21	7.66	7.78	0.39	0.12	0.25	6.89	4.36	0.03	0.51	98.63
76	PANTELLERIA, GEO, LdV, (Francaviglia, 1999)	66.59	0.64	11.41	7.58	0.30	0.00	0.65	7.58	4.46	0.04	0.07	99.31
77	PANTELLERIA, GEO, Mursia, (Francaviglia, 1999)	69.65	0.51	11.40	5.71	0.25	0.00	0.41	6.51	4.50	0.03	0.10	99.07
78	PANTELLERIA, GEO, Sciuvechi, (Francaviglia, 1999)	71.07	0.24	7.73	7.67	0.28	0.00	0.30	7.24	4.11	0.03	0.13	98.80
79	PANTELLERIA, GEO, BDT, (Francaviglia, 1999)	71.15	0.25	7.80	7.85	0.29	0.00	0.31	7.16	4.21	0.03	0.13	99.18
80	PANTELLERIA, ARCH, 1-Uzzo, (Francaviglia and Piperno, 1987)	66.34	0.62	10.49	8.05	0.30	0.18	0.70	7.40	4.50	0.04	0.09	98.71
81	PANTELLERIA, ARCH, 2-Uzzo, (Francaviglia and Piperno, 1987)	70.45	0.23	7.73	7.67	0.27	0.08	0.36	7.09	4.14	0.03	0.16	98.21
82	PANTELLERIA, ARCH, 1-Cofa_ (Francaviglia and Piperno, 1987)	69.52	0.29	7.78	8.38	0.29	0.26	0.53	6.90	4.09	0.04	0.20	98.28
83	PANTELLERIA, ARCH, 2-Cofa, (Francaviglia and Piperno, 1987)	69.40	0.26	7.49	9.55	0.33	0.11	0.37	6.40	4.51	0.30	0.20	98.92

No.	Source, Type, Location, Author	SiO_2	TiO_2	Al_2O_3	FeOtot	MnO	MgO	CaO	Na_2O	K_2O	P_2O_5	Cl	Tot%
84	PANTELLERIA, GEO, BDT, (Francaviglia, 1988)	70.35	0.25	7.86	8.60	0.30	0.09	0.33	6.84	4.38	0.02	0.23	99.25
85	PANTELLERIA, GEO, LdV, (Francaviglia, 1988)	69.45	0.51	10.94	6.02	0.26	0.23	0.41	6.32	4.70	0.03	0.16	99.03
86	PANTELLERIA, ARCH, Gelk, (Francaviglia, 1988)	66.26	0.64	10.94	8.34	0.31	0.20	0.64	7.04	4.70	0.04	0.12	99.23
87	PANTELLERIA, GEO, LdV-Sciuv, (Francaviglia, 1988)	70.72	0.24	7.68	8.16	0.29	0.09	0.29	6.91	4.20	0.02	0.22	98.82
88	PANTELLERIA, GEO, Up-Bdt, (Francaviglia, 1984)	70.83	0.24	7.72	8.20	0.29	0.08	0.29	6.93	4.25	0.02	0.22	99.07
89	PANTELLERIA, GEO, (Francaviglia, 1984)	71.65	0.23	7.60	8.51	0.28	0.09	0.30	6.86	4.29	0.03	0.34	100.18
90	PANTELLERIA, GEO, (MacDonald and Bailey, 1973)	68.60	0.65	10.64	6.18	0.27	0.45	0.49	6.36	4.80	0.05	0.35	98.84
91	PANTELLERIA, GEO, (MacDonald and Bailey, 1973)	68.00	0.65	11.34	5.26	0.21	0.45	0.53	7.76	4.72	0.06	0.51	99.49

Table 4/d. Lipari.

No.	Source, Type, Location, Author	SiO_2	TiO_2	Al_2O_3	FeOtot	MnO	MgO	CaO	Na_2O	K_2O	P_2O_5	Cl	Tot%
92	LIPARI, GEO, 1-Gabellotto, (Foresta Martin et al., 2020)	74.88	0.08	12.75	1.49	0.07	0.03	0.71	4.03	5.40	0.01	0.36	99.81
93	LIPARI, GEO, 2-Gabellotto, (Foresta Martin et al., 2020)	74.79	0.07	12.75	1.57	0.05	0.04	0.72	4.08	5.38	0.01	0.35	99.81
94	LIPARI, GEO, 3-Gabellotto, (Foresta Martin et al., 2020)	75.09	0.07	12.64	1.51	0.05	0.04	0.71	4.00	5.34	0.01	0.36	99.82
95	LIPARI, GEO, 1-Canneto D., (Foresta Martin et al., 2020)	75.23	0.05	12.62	1.44	0.07	0.04	0.68	3.98	5.38	0.02	0.33	99.84
96	LIPARI, GEO, 2-Canneto D., (Foresta Martin et al., 2020)	74.79	0.08	12.86	1.48	0.07	0.03	0.70	4.16	5.29	0.01	0.36	99.83
97	LIPARI, GEO, 3-Canneto D., (Foresta Martin et al., 2020)	74.84	0.08	12.80	1.51	0.06	0.05	0.72	4.10	5.29	0.02	0.34	99.81
98	LIPARI, ARCH, 1-Ust., (Foresta Martin et al., 2017)	75.24	0.13	13.24	1.51	0.10	0.11	0.75	4.17	5.20	0.04	0.33	100.82
99	LIPARI, ARCH, 2-Ust., (Foresta Martin et al., 2017)	74.68	0.03	13.21	1.42	0.10	0.09	0.69	4.05	5.11	0.03	0.31	99.72
100	LIPARI, ARCH, 3-Ust., (Foresta Martin et al., 2017)	74.72	0.11	13.21	1.47	0.06	0.10	0.66	4.03	4.99	0.00	0.33	99.68
101	LIPARI, ARCH, 4-Ust., (Foresta Martin et al., 2017)	75.53	0.11	13.27	1.47	0.06	0.11	0.69	4.23	5.16	0.02	0.29	100.94
102	LIPARI, ARCH, 5-Ust., (Foresta Martin et al., 2017)	75.39	0.10	13.29	1.36	0.08	0.11	0.63	4.22	5.14	0.03	0.31	100.66
103	LIPARI, ARCH, 7-Ust., (Foresta Martin et al., 2017)	74.96	0.06	13.20	1.38	0.04	0.14	0.64	3.99	5.17	0.03	0.29	99.90

No.	Source, Type, Location, Author	SiO_2	TiO_2	Al_2O_3	FeOtot	MnO	MgO	CaO	Na_2O	K_2O	P_2O_5	Cl	Tot%
104	LIPARI, ARCH, 8-Ust., (Foresta Martin et al., 2017)	75.14	0.10	13.09	1.40	0.09	0.14	0.75	4.21	5.08	0.01	0.30	100.31
105	LIPARI, ARCH, 9-Ust., (Foresta Martin et al., 2017)	75.25	0.08	13.15	1.50	0.10	0.14	0.70	4.14	5.11	0.03	0.31	100.51
106	LIPARI, ARCH, 11-Ust., (Foresta Martin et al., 2017)	74.62	0.14	12.95	1.49	0.07	0.12	0.64	4.06	5.00	0.00	0.33	99.42
107	LIPARI, ARCH, 12-Ust., (Foresta Martin et al., 2017)	74.39	0.06	12.98	1.46	0.07	0.10	0.67	4.05	5.12	0.03	0.31	99.24
108	LIPARI, ARCH, 13-Ust., (Foresta Martin et al., 2017)	75.15	0.08	12.94	1.38	0.06	0.07	0.66	4.03	4.87	0.07	0.33	99.64
109	LIPARI, ARCH, 14-Ust., (Foresta Martin et al., 2017)	75.04	0.09	13.04	1.47	0.07	0.13	0.70	4.12	5.08	0.04	0.30	100.08
110	LIPARI, ARCH, 15-Ust., (Foresta Martin et al., 2017)	74.50	0.08	12.97	1.51	0.05	0.08	0.74	4.17	5.08	0.05	0.32	99.55
111	LIPARI, ARCH, 16-Ust., (Foresta Martin et al., 2017)	74.79	0.14	13.15	1.56	0.07	0.14	0.74	4.13	5.08	0.05	0.32	100.17
112	LIPARI, ARCH, 17-Ust., (Foresta Martin et al., 2017)	75.92	0.09	13.25	1.40	0.10	0.14	0.68	4.09	5.17	0.02	0.30	101.16
113	LIPARI, ARCH, 19-Ust., (Foresta Martin et al., 2017)	74.99	0.09	13.15	1.50	0.08	0.13	0.71	4.07	5.04	0.02	0.31	100.09
114	LIPARI, ARCH, 20-Ust., (Foresta Martin et al., 2017)	75.56	0.11	12.84	1.44	0.06	0.10	0.66	3.67	5.40	0.02	0.30	100.16
115	LIPARI, ARCH, 22-Ust., (Foresta Martin et al., 2017)	74.82	0.08	12.96	1.45	0.09	0.12	0.68	4.02	5.07	0.02	0.32	99.63
116	LIPARI, ARCH, 23-Ust., (Foresta Martin et al., 2017)	74.48	0.07	12.99	1.55	0.06	0.14	0.70	4.08	5.25	0.03	0.33	99.68
117	LIPARI, ARCH, 24-Ust., (Foresta Martin et al., 2017)	75.08	0.12	13.05	1.43	0.06	0.09	0.72	4.10	5.13	0.03	0.31	100.12
118	LIPARI, ARCH, 25-Ust., (Foresta Martin et al., 2017)	75.24	0.05	13.08	1.44	0.11	0.10	0.74	4.12	5.13	0.01	0.32	100.34
119	LIPARI, ARCH, 26-Ust., (Foresta Martin et al., 2017)	75.38	0.11	13.15	1.43	0.05	0.11	0.71	4.13	4.97	0.04	0.29	100.37
120	LIPARI, ARCH, 27-Ust., (Foresta Martin et al., 2017)	75.40	0.09	13.19	1.55	0.09	0.13	0.75	4.15	5.12	0.02	0.31	100.80
121	LIPARI, ARCH, 28-Ust., (Foresta Martin et al., 2017)	75.50	0.10	13.25	1.41	0.14	0.10	0.75	4.06	5.12	0.05	0.30	100.78
122	LIPARI, ARCH, 29-Ust., (Foresta Martin et al., 2017)	75.29	0.07	13.12	1.50	0.05	0.10	0.70	4.01	5.01	0.04	0.33	100.22
123	LIPARI, ARCH, 30-Ust., (Foresta Martin et al., 2017)	75.58	0.07	13.13	1.46	0.07	0.12	0.76	4.05	5.06	0.03	0.29	100.62
124	LIPARI, ARCH, 31-Ust., (Foresta Martin et al., 2017)	75.21	0.10	13.30	1.47	0.07	0.10	0.74	4.13	5.06	0.02	0.32	100.52
125	LIPARI, ARCH, 32-Ust., (Foresta Martin et al., 2017)	75.95	0.09	13.09	1.40	0.10	0.08	0.68	4.03	5.06	0.03	0.33	100.84

No.	Source, Type, Location, Author	SiO_2	TiO_2	Al_2O_3	FeOtot	MnO	MgO	CaO	Na_2O	K_2O	P_2O_5	Cl	Tot%
126	LIPARI, ARCH, 34-Ust., (Foresta Martin et al., 2017)	74.67	0.09	13.13	1.46	0.07	0.15	0.72	3.98	5.03	0.06	0.30	99.66
127	LIPARI, ARCH, 35-Ust., (Foresta Martin et al., 2017)	75.89	0.11	13.23	1.19	0.07	0.09	0.69	3.96	5.34	0.03	0.28	100.88
128	LIPARI, ARCH, 36-Ust., (Foresta Martin et al., 2017)	76.03	0.12	13.30	1.47	0.06	0.11	0.71	4.18	5.03	0.02	0.30	101.33
129	LIPARI, ARCH, 37-Ust., (Foresta Martin et al., 2017)	75.00	0.10	13.02	1.54	0.09	0.13	0.71	4.07	4.90	0.05	0.34	99.95
130	LIPARI, ARCH, 38-Ust., (Foresta Martin et al., 2017)	74.70	0.08	12.98	1.53	0.07	0.08	0.69	4.03	5.11	0.01	0.35	99.63
131	LIPARI, ARCH, 39-Ust., (Foresta Martin et al., 2017)	76.01	0.06	12.88	1.38	0.08	0.10	0.66	3.97	5.16	0.03	0.33	100.66
132	LIPARI, ARCH, 41-Ust., (Foresta Martin et al., 2017)	75.37	0.08	13.21	1.45	0.06	0.12	0.72	4.06	5.02	0.01	0.31	100.41
133	LIPARI, ARCH, 42-Ust., (Foresta Martin et al., 2017)	76.19	0.10	13.29	1.13	0.06	0.11	0.63	4.13	5.36	0.07	0.29	101.36
134	LIPARI, ARCH, 43-Ust., (Foresta Martin et al., 2017)	75.46	0.14	13.02	1.50	0.10	0.09	0.71	3.84	5.61	0.02	0.32	100.81
135	LIPARI, ARCH, 44-Ust., (Foresta Martin et al., 2017)	76.06	0.09	13.37	1.45	0.06	0.09	0.68	4.20	5.11	0.03	0.32	101.46
136	LIPARI, ARCH, 45-Ust., (Foresta Martin et al., 2017)	75.84	0.08	13.27	1.46	0.05	0.14	0.67	4.13	5.20	-	0.30	101.14
137	LIPARI, ARCH, 46-Ust., (Foresta Martin et al., 2017)	75.58	0.10	13.14	1.44	0.06	0.12	0.75	3.93	5.37	0.02	0.33	100.84
138	LIPARI, ARCH, 47-Ust., (Foresta Martin et al., 2017)	76.29	0.16	13.20	1.57	0.11	0.09	0.74	4.24	5.09	0.02	0.34	101.85
139	LIPARI, ARCH, 50-Ust., (Foresta Martin et al., 2017)	76.07	0.09	13.13	1.48	0.04	0.12	0.72	4.01	5.00	0.04	0.32	101.02
140	LIPARI, ARCH, 51-Ust., (Foresta Martin et al., 2017)	74.68	0.06	13.10	1.42	0.08	0.11	0.67	3.90	5.28	0.04	0.30	99.64
141	LIPARI, ARCH, 52-Ust., (Foresta Martin et al., 2017)	75.14	0.04	13.10	1.48	0.15	0.11	0.70	3.93	5.12	—	0.31	100.08
142	LIPARI, ARCH, 53-Ust., (Foresta Martin et al., 2017)	74.71	0.06	13.13	1.46	0.12	0.10	0.71	3.96	5.15	0.02	0.30	99.72
143	LIPARI, ARCH, 54-Ust., (Foresta Martin et al., 2017)	75.23	0.13	13.02	1.45	0.06	0.10	0.66	3.93	5.13	0.03	0.30	100.04
144	LIPARI, ARCH, 55-Ust., (Foresta Martin et al., 2017)	74.59	0.11	12.95	1.50	0.10	0.09	0.71	4.01	5.13	0.02	0.27	99.48
145	LIPARI, ARCH, 57-Ust., (Foresta Martin et al., 2017)	74.37	0.10	12.79	1.50	0.09	0.12	0.68	3.92	5.11	0.04	0.30	99.02
146	LIPARI, ARCH, 58-Ust., (Foresta Martin et al., 2017)	74.96	0.07	13.09	1.37	0.08	0.07	0.69	4.01	5.13	0.05	0.31	99.83
147	LIPARI, ARCH, 59-Ust., (Foresta Martin et al., 2017)	75.14	0.13	13.00	1.47	0.07	0.10	0.69	3.99	5.15	0.04	0.32	100.10

No.	Source, Type, Location, Author	SiO_2	TiO_2	Al_2O_3	FeOtot	MnO	MgO	CaO	Na_2O	K_2O	P_2O_5	Cl	Tot%
148	LIPARI, ARCH, 60-Ust., (Foresta Martin et al., 2017)	74.60	0.12	12.98	1.47	0.05	0.10	0.73	4.03	5.06	0.02	0.34	99.50
149	LIPARI, ARCH, 62-Ust., (Foresta Martin et al., 2017)	74.97	0.12	13.00	1.49	0.07	0.10	0.73	3.92	5.06	0.00	0.33	99.79
150	LIPARI, ARCH, 63-Ust., (Foresta Martin et al., 2017)	75.39	0.06	12.91	1.43	0.10	0.10	0.69	3.91	5.14	0.02	0.29	100.04
151	LIPARI, ARCH, 64-Ust., (Foresta Martin et al., 2017)	75.03	0.06	12.93	1.36	0.11	0.10	0.68	3.98	5.18	0.02	0.29	99.74
152	LIPARI, ARCH, 65-Ust., (Foresta Martin et al., 2017)	74.93	0.11	12.93	1.50	0.02	0.12	0.67	3.98	5.14	0.05	0.31	99.76
153	LIPARI, ARCH, 66-Ust., (Foresta Martin et al., 2017)	75.18	0.10	13.10	1.46	0.05	0.11	0.72	4.04	5.24	0.03	0.30	100.33
154	LIPARI, ARCH, 67-Ust., (Foresta Martin et al., 2017)	75.14	0.04	12.96	1.54	0.04	0.09	0.67	4.00	5.12	0.05	0.28	99.93
155	LIPARI, ARCH, 68-Ust., (Foresta Martin et al., 2017)	75.27	0.15	13.11	1.40	0.07	0.08	0.69	3.92	5.18	0.03	0.28	100.18
156	LIPARI, ARCH, 70-Ust., (Foresta Martin et al., 2017)	75.23	0.12	12.98	1.35	0.06	0.10	0.71	3.85	5.37	0.01	0.31	100.09
157	LIPARI, ARCH, 71-Ust., (Foresta Martin et al., 2017)	75.72	0.10	13.11	1.52	0.07	0.10	0.67	4.05	5.24	0.02	0.30	100.90
158	LIPARI, ARCH, 72-Ust., (Foresta Martin et al., 2017)	74.82	0.11	12.92	1.53	0.10	0.12	0.72	4.01	5.05	0.03	0.32	99.73
159	LIPARI, ARCH, 73-Ust., (Foresta Martin et al., 2017)	75.07	0.11	13.00	1.49	0.08	0.12	0.72	3.90	5.34	0.02	0.31	100.16
160	LIPARI, ARCH, 74-Ust., (Foresta Martin et al., 2017)	75.35	0.08	13.00	1.53	0.07	0.11	0.71	4.00	5.11	0.02	0.33	100.31
161	LIPARI, ARCH, 75-Ust., (Foresta Martin et al., 2017)	74.90	0.09	13.04	1.47	0.11	0.13	0.75	4.00	5.16	0.01	0.28	99.94
162	LIPARI, ARCH, 76-Ust., (Foresta Martin et al., 2017)	75.01	0.11	12.89	1.59	0.05	0.12	0.70	3.92	5.24	0.03	0.32	99.98
163	LIPARI, ARCH, 79-Ust., (Foresta Martin et al., 2017)	75.23	0.11	12.91	1.48	0.05	0.10	0.70	3.91	5.06	0.04	0.30	99.89
164	LIPARI, ARCH, 81-Ust., (Foresta Martin et al., 2017)	75.03	0.10	12.69	1.34	0.04	0.10	0.70	3.84	5.01	0.02	0.29	99.16
165	LIPARI, ARCH, 83-Ust., (Foresta Martin et al., 2017)	74.59	0.06	12.86	1.41	0.08	0.11	0.72	3.98	5.02	0.02	0.31	99.16
166	LIPARI, ARCH, 84-Ust., (Foresta Martin et al., 2017)	74.06	0.12	12.93	1.52	0.10	0.08	0.71	3.89	5.07	0.02	0.30	98.80
167	LIPARI, ARCH, 86-Ust., (Foresta Martin et al., 2017)	74.86	0.06	12.93	1.48	0.03	0.11	0.72	3.91	5.17	0.01	0.31	99.59
168	LIPARI, ARCH, 87-Ust., (Foresta Martin et al., 2017)	75.58	0.09	12.87	1.47	0.09	0.09	0.71	3.88	5.15	0.02	0.30	100.25
169	LIPARI, ARCH, 88-Ust., (Foresta Martin et al., 2017)	75.16	0.11	12.90	1.45	0.09	0.11	0.72	3.99	5.01	0.03	0.32	99.89

No.	Source, Type, Location, Author	SiO_2	TiO_2	Al_2O_3	FeOtot	MnO	MgO	CaO	Na_2O	K_2O	P_2O_5	Cl	Tot%
170	LIPARI, ARCH, 89-Ust., (Foresta Martin et al., 2017)	75.04	0.12	13.00	1.39	0.11	0.09	0.73	4.02	5.07	0.03	0.30	99.90
171	LIPARI, ARCH, 90-Ust., (Foresta Martin et al., 2017)	75.06	0.08	13.12	1.48	0.10	0.09	0.73	3.90	5.13	0.00	0.31	100.00
172	LIPARI, ARCH, 91-Ust., (Foresta Martin et al., 2017)	74.91	0.10	12.92	1.42	0.09	0.11	0.68	3.91	5.09	–	0.29	99.52
173	LIPARI, ARCH, 92-Ust., (Foresta Martin et al., 2017)	74.66	0.10	12.97	1.48	0.05	0.12	0.69	3.86	5.29	0.03	0.33	99.58
174	LIPARI, ARCH, 93-Ust., (Foresta Martin et al., 2017)	75.08	0.10	12.84	1.51	0.09	0.13	0.68	3.90	5.26	0.02	0.30	99.91
175	LIPARI, ARCH, 94-Ust., (Foresta Martin et al., 2017)	74.67	0.10	12.84	1.47	0.04	0.12	0.70	3.90	5.12	0.01	0.31	99.28
176	LIPARI, ARCH, 95-Ust., (Foresta Martin et al., 2017)	74.32	0.12	12.90	1.50	0.14	0.09	0.70	3.78	5.09	0.06	0.30	99.00
177	LIPARI, ARCH, 97-Ust., (Foresta Martin et al., 2017)	75.13	0.07	12.96	1.28	0.13	0.11	0.68	4.03	5.20	0.02	0.28	99.89
178	LIPARI, ARCH, 98-Ust., (Foresta Martin et al., 2017)	75.60	0.08	12.96	1.41	0.05	0.12	0.69	4.00	5.19	0.05	0.30	100.45
179	LIPARI, ARCH, 99-Ust., (Foresta Martin et al., 2017)	75.10	0.06	12.80	1.48	0.11	0.12	0.72	3.97	5.16	0.02	0.31	99.85
180	LIPARI, ARCH, 100-Ust., (Foresta Martin et al., 2017)	75.35	0.14	12.96	1.39	0.08	0.08	0.66	3.90	5.30	0.03	0.31	100.20
181	LIPARI, ARCH, 101-Ust., (Foresta Martin et al., 2017)	75.87	0.09	13.21	1.39	0.04	0.11	0.78	4.03	5.06	0.03	0.33	100.94
182	LIPARI, ARCH, 102-Ust., (Foresta Martin et al., 2017)	76.34	0.13	13.34	1.32	0.04	0.13	0.65	3.74	5.97	0.01	0.29	101.96
183	LIPARI, ARCH, 103-Ust., (Foresta Martin et al., 2017)	75.07	0.07	13.17	1.54	0.09	0.12	0.69	4.02	5.03	0.04	0.30	100.14
184	LIPARI, ARCH, 105-Ust., (Foresta Martin et al., 2017)	76.30	0.08	13.06	1.53	0.10	0.12	0.66	4.07	5.20	0.03	0.31	101.46
185	LIPARI, ARCH, 106-Ust., (Foresta Martin et al., 2017)	75.73	0.09	13.33	1.50	0.08	0.09	0.72	4.11	5.14	0.02	0.32	101.13
186	LIPARI, ARCH, 107-Ust., (Foresta Martin et al., 2017)	75.09	0.04	12.98	1.38	0.12	0.10	0.61	4.00	5.18	0.04	0.32	99.86
187	LIPARI, ARCH, 108-Ust., (Foresta Martin et al., 2017)	75.63	0.08	13.17	1.48	0.06	0.12	0.74	4.13	5.11	0.04	0.32	100.88
188	LIPARI, ARCH, 109-Ust., (Foresta Martin et al., 2017)	75.54	0.08	13.39	1.45	0.06	0.09	0.71	4.27	4.99	–	0.32	100.90
189	LIPARI, ARCH, 110-Ust., (Foresta Martin et al., 2017)	75.78	0.13	13.23	1.50	0.10	0.12	0.70	4.05	5.28	0.03	0.31	101.23
190	LIPARI, ARCH, 111-Ust., (Foresta Martin et al., 2017)	75.73	0.12	13.14	1.45	0.09	0.09	0.69	4.07	5.06	0.03	0.31	100.78
191	LIPARI, ARCH, 113-Ust., (Foresta Martin et al., 2017)	75.69	0.06	13.33	1.35	0.14	0.12	0.71	4.01	5.07	0.00	0.29	100.77

No.	Source, Type, Location, Author	SiO_2	TiO_2	Al_2O_3	FeOtot	MnO	MgO	CaO	Na_2O	K_2O	P_2O_5	Cl	Tot%
192	LIPARI, ARCH, 114-Ust., (Foresta Martin et al., 2017)	75.39	0.08	12.91	1.41	0.08	0.11	0.69	4.05	5.23	0.04	0.32	100.31
193	LIPARI, ARCH, 115-Ust., (Foresta Martin et al., 2017)	75.58	0.08	13.14	1.48	0.07	0.09	0.70	4.06	5.05	0.04	0.30	100.59
194	LIPARI, ARCH, 116-Ust., (Foresta Martin et al., 2017)	75.11	0.09	13.23	1.45	0.12	0.10	0.70	4.14	5.04	0.02	0.32	100.32
195	LIPARI, ARCH, 117-Ust., (Foresta Martin et al., 2017)	74.87	0.04	13.11	1.33	0.06	0.11	0.67	4.06	5.08	0.02	0.29	99.64
196	LIPARI, ARCH, 118-Ust., (Foresta Martin et al., 2017)	75.18	0.08	13.23	1.48	0.09	0.12	0.73	4.10	5.09	0.03	0.33	100.46
197	LIPARI, ARCH, 119-Ust., (Foresta Martin et al., 2017)	75.33	0.08	13.20	1.43	0.08	0.11	0.72	4.13	5.17	0.05	0.31	100.61
198	LIPARI, ARCH, 120-Ust., (Foresta Martin et al., 2017)	75.34	0.11	12.96	1.24	0.08	0.09	0.66	4.04	5.17	0.03	0.33	100.05
199	LIPARI, ARCH, 121-Ust., (Foresta Martin et al., 2017)	75.01	0.11	13.20	1.54	0.12	0.10	0.64	4.05	5.08	0.03	0.31	100.19
200	LIPARI, ARCH, 122-Ust., (Foresta Martin et al., 2017)	75.04	0.09	13.17	1.46	0.05	0.08	0.73	4.11	5.13	0.00	0.30	100.16
201	LIPARI, ARCH, 123-Ust., (Foresta Martin et al., 2017)	75.05	0.06	13.09	1.28	0.08	0.09	0.68	3.99	5.06	0.02	0.29	99.69
202	LIPARI, ARCH, 124-Ust., (Foresta Martin et al., 2017)	73.77	0.10	13.07	1.49	0.07	0.12	0.69	4.02	4.95	0.04	0.32	98.64
203	LIPARI, ARCH, 125-Ust., (Foresta Martin et al., 2017)	73.26	0.09	12.90	1.43	0.07	0.10	0.70	3.96	4.97	—	0.30	97.78
204	LIPARI, ARCH, 127-Ust., (Foresta Martin et al., 2017)	74.40	0.10	12.87	1.50	0.06	0.11	0.73	3.92	4.97	0.05	0.32	99.03
205	LIPARI, ARCH, 128-Ust., (Foresta Martin et al., 2017)	75.19	0.12	12.83	1.46	0.06	0.11	0.69	4.00	5.15	—	0.31	99.92
206	LIPARI, ARCH, 129-Ust., (Foresta Martin et al., 2017)	75.30	0.08	13.02	1.48	0.06	0.12	0.75	4.02	5.15	0.01	0.29	100.28
207	LIPARI, ARCH, 130-Ust., (Foresta Martin et al., 2017)	74.65	0.07	13.02	1.50	0.09	0.13	0.72	3.85	5.09	0.02	0.31	99.45
208	LIPARI, ARCH, 131-Ust., (Foresta Martin et al., 2017)	74.63	0.10	12.87	1.48	0.07	0.10	0.72	3.96	5.07	0.01	0.31	99.32
209	LIPARI, ARCH, 132-Ust., (Foresta Martin et al., 2017)	75.11	0.10	13.03	1.43	0.12	0.09	0.69	4.00	5.19	0.06	0.28	100.10
210	LIPARI, ARCH, 133-Ust., (Foresta Martin et al., 2017)	75.13	0.11	12.95	1.24	0.09	0.11	0.68	3.99	5.17	0.01	0.25	99.73
211	LIPARI, ARCH, 134-Ust., (Foresta Martin et al., 2017)	74.78	0.07	12.91	1.43	0.07	0.09	0.71	3.90	5.22	0.03	0.30	99.51
212	LIPARI, ARCH, 135-Ust., (Foresta Martin et al., 2017)	74.92	0.10	12.91	1.32	0.07	0.11	0.66	3.84	5.16	0.03	0.29	99.41
213	LIPARI, ARCH, 136-Ust., (Foresta Martin et al., 2017)	74.91	0.10	13.11	1.49	0.10	0.10	0.72	4.04	5.10	0.06	0.34	100.07

No.	Source, Type, Location, Author	SiO_2	TiO_2	Al_2O_3	FeOtot	MnO	MgO	CaO	Na_2O	K_2O	P_2O_5	Cl	Tot%
214	LIPARI, ARCH, 138-Ust., (Foresta Martin et al., 2017)	74.39	0.08	12.89	1.55	0.06	0.10	0.75	3.95	5.22	–	0.30	99.29
215	LIPARI, ARCH, 139-Ust., (Foresta Martin et al., 2017)	74.24	0.10	12.94	1.49	0.08	0.13	0.70	4.08	5.14	0.05	0.29	99.24
216	LIPARI, ARCH, 140-Ust., (Foresta Martin et al., 2017)	74.15	0.07	12.91	1.56	0.08	0.08	0.67	3.94	5.12	–	0.33	98.91
217	LIPARI, ARCH, 141-Ust., (Foresta Martin et al., 2017)	74.57	0.06	13.11	1.27	0.08	0.11	0.68	4.01	5.18	0.02	0.25	99.34
218	LIPARI, ARCH, 142-Ust., (Foresta Martin et al., 2017)	73.95	0.12	12.74	1.31	0.07	0.15	0.71	3.87	5.06	0.02	0.32	98.32
219	LIPARI, ARCH, 143-Ust., (Foresta Martin et al., 2017)	73.92	0.12	13.02	1.48	0.09	0.12	0.64	3.93	5.10	0.03	0.31	98.76
220	LIPARI, ARCH, 144-Ust., (Foresta Martin et al., 2017)	74.56	0.07	12.97	1.44	0.08	0.09	0.68	3.79	5.14	0.04	0.32	99.18
221	LIPARI, ARCH, 145-Ust., (Foresta Martin et al., 2017)	74.71	0.09	12.92	1.31	0.07	0.12	0.67	4.00	5.13	0.01	0.30	99.33
222	LIPARI, ARCH, 146-Ust., (Foresta Martin et al., 2017)	74.35	0.11	12.99	1.49	0.07	0.09	0.68	3.67	5.76	0.04	0.30	99.55
223	LIPARI, ARCH, 147-Ust., (Foresta Martin et al., 2017)	73.90	0.07	12.91	1.51	0.08	0.08	0.68	3.99	5.06	0.03	0.32	98.63
224	LIPARI, ARCH, 148-Ust., (Foresta Martin et al., 2017)	74.63	0.11	12.74	1.41	0.04	0.10	0.76	3.69	5.47	0.07	0.31	99.33
225	LIPARI, ARCH, 149-Ust., (Foresta Martin et al., 2017)	74.76	0.11	12.78	1.46	0.06	0.10	0.69	3.98	5.07	0.05	0.30	99.36
226	LIPARI, ARCH, 150-Ust., (Foresta Martin et al., 2017)	74.41	0.12	12.81	1.33	0.10	0.08	0.70	3.81	5.20	0.05	0.29	98.90
227	LIPARI, ARCH, 151-Ust., (Foresta Martin et al., 2017)	75.26	0.14	13.00	1.35	0.10	0.12	0.70	3.89	5.11	0.04	0.32	100.03
228	LIPARI, ARCH, 152-Ust., (Foresta Martin et al., 2017)	74.08	0.08	12.78	1.48	0.08	0.09	0.69	3.93	5.08	0.01	0.34	98.64
229	LIPARI, ARCH, 154-Ust., (Foresta Martin et al., 2017)	74.72	0.12	13.09	1.34	0.05	0.12	0.62	3.93	5.19	0.00	0.29	99.47
230	LIPARI, ARCH, 155-Ust., (Foresta Martin et al., 2017)	74.54	0.10	12.84	1.27	0.07	0.10	0.67	3.87	5.10	0.05	0.29	98.90
231	LIPARI, ARCH, 156-Ust., (Foresta Martin et al., 2017)	73.89	0.04	12.63	1.17	0.07	0.10	0.49	3.94	4.99	0.04	0.34	97.70
232	LIPARI, ARCH, 157-Ust., (Foresta Martin et al., 2017)	74.74	0.09	13.07	1.41	0.07	0.10	0.68	3.96	5.18	0.02	0.31	99.63
233	LIPARI, ARCH, 158-Ust., (Foresta Martin et al., 2017)	74.23	0.06	12.88	1.54	0.10	0.09	0.67	4.00	5.15	0.04	0.30	99.06
234	LIPARI, ARCH, 159-Ust., (Foresta Martin et al., 2017)	74.45	0.10	13.04	1.53	0.06	0.08	0.64	3.86	5.48	0.01	0.31	99.56
235	LIPARI, ARCH, 160-Ust., (Foresta Martin et al., 2017)	74.12	0.08	13.06	1.49	0.10	0.12	0.72	3.94	5.05	0.02	0.31	99.01

No.	Source, Type, Location, Author	SiO_2	TiO_2	Al_2O_3	FeOtot	MnO	MgO	CaO	Na_2O	K_2O	P_2O_5	Cl	Tot%
236	LIPARI, ARCH, 161-Ust., (Foresta Martin et al., 2017)	75.03	0.10	12.82	1.58	0.08	0.10	0.73	3.96	5.17	0.04	0.34	99.95
237	LIPARI, ARCH, 162-Ust., (Foresta Martin et al., 2017)	74.47	0.08	12.84	1.49	0.09	0.07	0.67	3.90	5.30	0.03	0.32	99.26
238	LIPARI, ARCH, 163-Ust., (Foresta Martin et al., 2017)	74.39	0.09	12.87	1.33	0.06	0.11	0.72	3.90	5.06	—	0.33	98.86
239	LIPARI, ARCH, 164-Ust., (Foresta Martin et al., 2017)	74.21	0.09	12.89	1.52	0.05	0.11	0.79	3.95	5.13	0.03	0.32	99.09
240	LIPARI, ARCH, 166-Ust., (Foresta Martin et al., 2017)	74.22	0.11	12.95	1.48	0.05	0.11	0.72	4.05	5.00	0.04	0.31	99.04
241	LIPARI, ARCH, 167-Ust., (Foresta Martin et al., 2017)	74.19	0.09	13.03	1.55	0.06	0.12	0.73	3.99	5.05	0.01	0.32	99.14
242	LIPARI, ARCH, 168-Ust., (Foresta Martin et al., 2017)	74.82	0.10	13.17	1.51	0.10	0.11	0.74	3.97	5.06	0.01	0.31	99.90
243	LIPARI, ARCH, 169-Ust., (Foresta Martin et al., 2017)	74.40	0.11	12.83	1.42	0.07	0.09	0.68	3.94	5.09	0.04	0.30	98.97
244	LIPARI, ARCH, 170-Ust., (Foresta Martin et al., 2017)	74.52	0.12	12.78	1.34	0.10	0.10	0.67	4.05	5.28	0.02	0.30	99.28
245	LIPARI, ARCH, 171-Ust., (Foresta Martin et al., 2017)	74.30	0.12	12.76	1.44	0.13	0.11	0.70	3.93	5.13	0.04	0.30	98.96
246	LIPARI, ARCH, 172-Ust., (Foresta Martin et al., 2017)	75.15	0.09	13.25	1.48	0.09	0.10	0.70	4.00	5.12	0.05	0.32	100.35
247	LIPARI, ARCH, 173-Ust., (Foresta Martin et al., 2017)	74.97	0.08	12.91	1.47	0.08	0.09	0.66	3.96	5.16	0.04	0.32	99.74
248	LIPARI, ARCH, 174-Ust., (Foresta Martin et al., 2017)	73.95	0.08	12.83	1.43	0.07	0.10	0.70	3.95	5.12	0.04	0.32	98.59
249	LIPARI, ARCH, 175-Ust., (Foresta Martin et al., 2017)	74.21	0.09	12.93	1.47	0.04	0.10	0.72	3.74	5.55	0.03	0.28	99.16
250	LIPARI, ARCH, (Kasztovszky et al., 2019)	73.90	0.08	13.20	1.63	0.07	0.00	0.77	4.33	5.19	0.00	0.33	99.50
251	LIPARI, GEO, Papesca, (Francaviglia, 1999)	74.21	0.09	12.47	1.99	0.07	0.00	0.64	4.36	5.39	0.01	0.05	99.28
252	LIPARI, ARCH, 3-Grotta Uzzo, (Francaviglia and Piperno, 1987)	73.53	0.09	12.56	1.77	0.07	0.08	0.82	4.52	4.90	0.02	0.10	98.46
253	LIPARI, ARCH, 4-Grotta Uzzo, (Francaviglia and Piperno, 1987)	70.71	0.09	12.19	1.66	0.06	0.07	1.47	4.40	4.65	0.03	0.10	95.43
254	LIPARI, ARCH, 5-Grotta Uzzo, (Francaviglia and Piperno, 1987)	71.45	0.08	12.38	1.76	0.06	0.08	0.72	4.46	4.66	0.02	0.10	95.77
255	LIPARI, ARCH, 2-M. Cofano, (Francaviglia and Piperno, 1987)	74.01	0.10	12.89	1.86	0.07	0.10	0.79	4.37	5.08	0.02	0.13	99.42
256	LIPARI, ARCH, 3-M. Cofano, (Francaviglia and Piperno, 1987)	73.32	0.10	12.32	2.74	0.08	0.11	0.85	4.06	5.56	0.03	0.13	99.30
257	LIPARI, GEO, Papesca, (Francaviglia, 1984)	74.10	0.07	13.23	1.65	0.08	0.11	0.71	4.24	4.86	0.03	0.23	99.31

No.	Source, Type, Location, Author	SiO_2	TiO_2	Al_2O_3	FeOtot	MnO	MgO	CaO	Na_2O	K_2O	P_2O_5	Cl	Tot%
258	LIPARI, GEO, Pom. Lam., (Francaviglia, 1984)	74.17	0.07	13.11	1.62	0.08	0.10	0.70	4.12	4.86	0.10	0.23	99.16
259	LIPARI, GEO, Pap. FoV., (Francaviglia, 1984)	74.08	0.07	13.24	1.68	0.08	0.11	0.72	4.17	4.90	0.03	0.23	99.31
260	LIPARI, GEO, Roc. Ros., (Francaviglia, 1984)	74.28	0.07	13.12	1.61	0.08	0.11	0.71	4.11	4.95	0.03	0.24	99.31
261	LIPARI, GEO, (MacDonald et al., 1992)	74.70	0.08	13.13	1.63	0.12	0.04	0.87	4.23	5.05	0.01	0.34	100.20
262	LIPARI, GEO, (MacDonald et al., 1992)	74.60	0.09	13.24	1.60	0.08	0.04	0.61	4.16	4.92	0.01	0.30	99.65

4. Seven discriminant diagrams to be compared

The assembled database was first used to compare the discriminating power of seven bivariate plots employed in obsidian provenance studies in the last decades. It is worth noting that the seven diagrams considered here, when applied to the obsidian assemblages analyzed by their respective authors, effectively fulfilled their task of discriminating geological sources. We now intend to test and compare their discriminatory ability on a composite assemblage consisting of obsidian samples collected and analyzed using various methods by different authors. The seven selected diagrams are listed below, adding for each one a review of their geochemical significance and the proposing authors. Let's follow a chronological order.

a) SiO_2 vs K_2O/Na_2O. In a seminal paper based on XRF analyses of over 500 obsidian samples from Italian and Greek Mediterranean sources, Francaviglia (1984) recommended the use of classical petrochemical methods for provenance studies and indicated the SiO2 vs K_2O/Na_2O bivariate plot as an effective identifier. K_2O/Na_2O is <1 for peralkaline (pantelleritic) obsidian, and >1 for the subalkaline sources (Palmarola, Lipari and Monte Arci, in an ideal increasing sequence), allowing – as the author points out – an almost complete discrimination of sources (Francaviglia, 1984).

b) $\sigma = (Na_2O + K_2O)^2/(SiO_2 - 43)$ vs $\tau = (Al_2O_3 - Na_2O)/(P_2O_5 + TiO_2)$. Sigma ($\sigma$) is the Rittmann Serial Index, originally introduced by Rittmann (1957, 1962) to quantify magmatic alkalinity and discriminate igneous rock series. Tau (τ) is the Gottini Index, first defined by Gottini (1968) as an empirical petrogenetic parameter aimed at capturing the relative evolution of volcanic magmas. The joint use of $\log\sigma$ versus $\log\tau$ was employed by Rittmann (1973) to distinguish orogenic and anorogenic volcanic series on a global dataset of ~1300 lavas. The use of σ vs τ diagram for effective discrimination of Mediterranean obsidian sources was then proposed at the end of the last century in many of the papers published by Francaviglia (1984, 1987, 1988, 1999).

c) SiO_2 vs CaO. The calcium plotted against silica was indicated by Tykot (2002) as one diagram employable when only major/minor elements are chosen as discriminants. Its effectiveness is due to the slightly increasing average calcium content that can be detected in the Pantelleria, Palmarola, Lipari and Monte Arci obsidians sequence. It is probably a simplified variant of the more complex CaO vs $SiO_2/(Na_2O + K_2O)$ diagram, introduced by Peacock (1931) and re-proposed by MacDonald et al. (1992) for classifying obsidians into calcic, calc-alkalic, and alkali-calcic.

d) Na_2O vs Al_2O_3. This binary diagram, adopted by Le Bourdonnec et al. (2010) to distinguish the four Italian obsidian sources, is based mainly on the increasing concentration of Na_2O that can be observed in the Monte Arci, Lipari, Palmarola and Pantelleria sequence. In the obsidian assemblage of Le Bourdonnec et al. (2010) Na_2O discrimination capacity was so evident that it was indicated as one of the main source selectors for Central Mediterranean obsidian sources.

e) $\log(SiO_2/Al_2O_3)$, vs $\log(CaO/Al_2O_3)$. Proposed by Orange et al. (2017), it expresses how much silica and calcium vary relative to the same, stable reference component (Al_2O_3). In practice, the horizontal axis of this diagram reflects how evolved or polymerized the glass is, while the vertical axis highlights differences linked to calcium-bearing minerals. Both aspects discriminate volcanic glasses, because different obsidian sources

tend to have different balances of silica, alumina and calcium. The logarithm of the ratios helps to separate the groups even more cleanly, because it corrects for the mathematical distortions that affect data expressed in percentages.

f) CaO/FeO_{tot} vs Cl. This diagram was originally formulated by Giaccio et al. (2017) for identifying the source of tephra from volcanoes of Campania and Latium Italian regions. In 2022, the use of this diagram for the studies of obsidian provenance was suggested by Ilenia Arienzo, co-author of Giaccio et al. (2017) paper, (personal communication). The diagram combines the selective aptitude of Cl, already proposed by Foresta Martin et al. (2019, 2020), with that of the CaO/FeO_{tot} ratio which increases in the sequence: Pantelleria, Palmarola, Lipari and Monte Arci.

g) Na_2O vs Cl. Proposed by Foresta Martin et al. (2019, 2020) for the clear discrimination of the four Central Mediterranean obsidian sources, this diagram owes its effectiveness to some peculiar Cl behaviors in the course of magmatic processes, as already mentioned in paragraph 2.1, i. e.: its relative incompatibility with crystalline phases, increasing concentration in the residual melts of evolved magmas, positive correlation with alkalis and sodium in particular.

An additional factor contributing to the superior performance of the Na_2O vs Cl system lies in the use of directly measured oxide concentrations rather than derived ratios or composite parameters. In ratio-based indices, analytical uncertainties propagate nonlinearly, potentially amplifying dispersion and increasing inter-source overlap. By contrast, bivariate spaces defined by independent elemental abundances tend to preserve the original analytical variance structure, resulting in more stable and interpretable discriminant fields. This consideration provides a further rationale for the robustness of the Na_2O vs Cl diagram observed in the comparative analysis.

4.1 Applying KDE + Mahalanobis statistics

Preliminary visual inspection shows that six out of the seven discriminant diagrams listed in the previous paragraph display partial overlap among the fields of the Central Mediterranean obsidian sources. To complement this qualitative overview, we aimed to provide a quantitative assessment of overlapping areas, inliers, and outliers for each diagram, using a consistent statistical procedure. Accordingly, the seven bivariate plots were subjected to a combined treatment based on Kernel Density Estimation (KDE) (Silverman, 1986) and Mahalanobis distance (Mahalanobis, 1936). KDE was used to reconstruct the empirical probability density of each source, while Mahalanobis distance enabled the identification of confidence ellipses and outliers (Fig. 5).

A bivariate Gaussian KDE was computed for each source using the global bandwidth defined by Scott's rule (Scott, 1979, 2015). Because all diagrams involve compositional variables constrained to positive values, a mirror boundary correction was applied, following common practice in geochemical KDE applications (e.g., Hyndman, 1996), to prevent edge depletion and produce a smooth, unbiased density estimate.

For each KDE surface, the global mode – the point of highest estimated density – was taken as the statistical centroid of the source. This "modal component", following the rationale described by Hyndman (1996) and Bowman and Azzalini (1997), provides a more robust measure of central tendency than the arithmetic mean, which is more sensitive to outliers and skewed distributions.

Mahalanobis distances were then calculated using the covariance matrix of each source. Confidence ellipses corresponding to the 97.5% χ^2 probability level (for 2 degrees of freedom) were generated, in accordance with common practice in multivariate archaeometric analysis. Points falling outside the 97.5% ellipse were classified as outliers. This confidence threshold was chosen because, as noted in several geochemical applications (e.g., Baxter, 2003), it provides a reliable balance between sensitivity and specificity, minimizing false positives while maintaining robust discriminant capability. Lower confidence levels (e.g., 90-95%) tend to contract confidence ellipses and artificially increase apparent inter-source overlap, whereas higher levels (e.g., 99%) disproportionately expand ellipses and inflate the number of outliers, particularly for sources represented by small sample sizes. Because the objective of this study is a comparative assessment of discriminant performance under uniform statistical conditions, a single confidence level was applied consistently across all diagrams.

After outliers were identified, KDE surfaces were recalculated using only inlier points, resulting in tighter and more statistically coherent clusters. No iterative exclusion-recalculation procedure was applied to avoid overfitting and to preserve the empirical nature of the distributions.

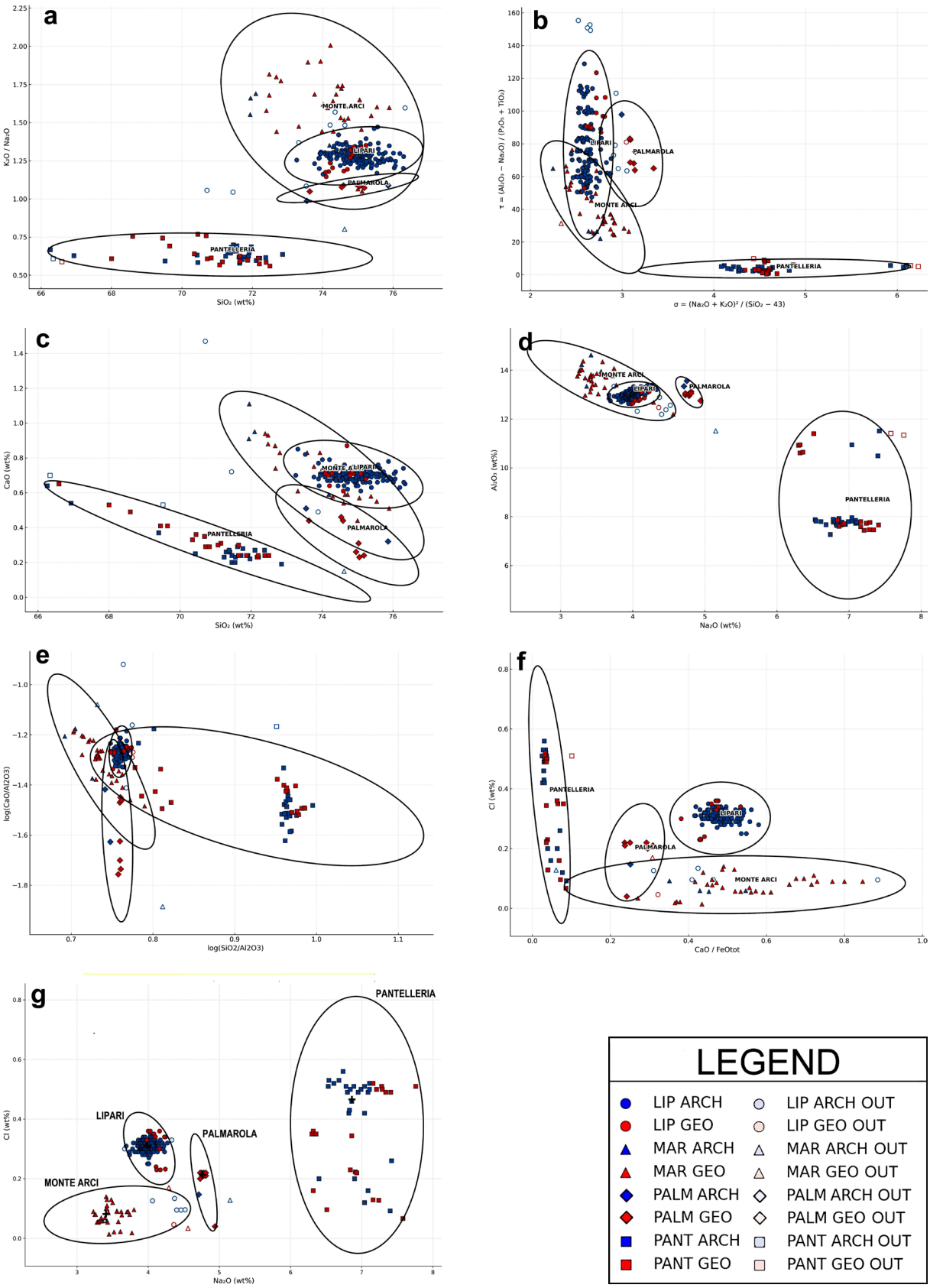

Figure 5. Mosaic of seven discriminating binary diagrams proposed in the literature, compared by means of KDE + Mahalanobis statistics. (a) SiO_2 vs K_2O/Na_2O. (b) $\sigma = (Na_2O + K_2O)^2/(SiO_2 - 43)$ vs $\tau = (Al_2O_3 - Na_2O)/(P_2O_5 + TiO_2)$. (c) SiO_2 vs CaO. (d) Na_2O vs Al_2O_3. (e) $\log(SiO_2/Al_2O_3)$, vs $\log(CaO/Al_2O_3)$. (f) CaO/FeOtot vs Cl. (g) Na_2O vs Cl. Red symbols = geologic samples; blue symbols = archaeologic. Empty red symbols = geologic outliers; empty blue symbols = archaeologic outliers.

The combined KDE + Mahalanobis approach therefore provides: (1) the statistical centroids of each source; (2) confidence ellipses describing their high-density regions; (3) objective identification of outliers; and (4) a quantitative assessment of inter-source separation in each bivariate compositional space considered.

For comparative purposes, the Mean % of ellipse overlap, Mean % of inliers, Mean % of outliers, and the Discriminant Power Index (DPI) were calculated for each of the seven bivariate systems. The areal overlap between the 97.5% Mahalanobis confidence ellipses of the four obsidian sources was quantified pairwise.

The intersection area between two ellipses (Aij) was estimated by Monte Carlo sampling of 50,000 random points within their joint bounding box. Overlap was defined as:

$$Overlap_{ij} = 100 \times \frac{A_{ij}}{0.5(A_i + A_j)} \quad (1)$$

using a strict '<' boundary criterion. The Mean % Overlap is the arithmetic mean of the six pairwise overlaps. Inliers were defined as points inside the 97.5% ellipse, and outliers as points outside it. The Discriminant Power Index was calculated as:

$$\text{DPI} = 100 - [(\text{Outliers mean}) + (\text{Overlap mean})] \quad (2)$$

where the Mean % Outliers is the average percentage of outliers across the four sources (according to the 97.5% Mahalanobis criterion), and the Mean % Overlap is the mean of the six pairwise ellipse overlaps. DPI ranges from 0 to 100, with higher values indicating diagrams that simultaneously exhibit tighter within-source clustering and lower inter-source overlap. The DPI is a composite, scale-free heuristic, intended exclusively for the relative ranking of discriminant performance among the seven bivariate systems tested under identical dataset and statistical conditions.

Multimodal density patterns observed in several source distributions may reflect a combination of geological and analytical factors. These include genuine heterogeneity within volcanic sources, such as the presence of sub-sources or compositional zoning, as well as inter-laboratory variability arising from differences in analytical techniques, calibration protocols, and detection limits. In addition, the aggregation of data derived from multiple published studies spanning several decades may further contribute to complex, non-unimodal distributions. Rather than being treated as noise or artifacts, such multimodality is explicitly accommodated by the KDE-based approach adopted here, which is designed to capture empirical probability densities without imposing unimodal assumptions.

5. Evaluating the best discrimination plots

Statistical analysis of the dataset carried out on the seven selected bivariate plots, and their graphical representations indicate that the four main Central Mediterranean obsidian sources tend to cluster in chemically distinct fields, but the respective confidence ellipses overlap to varying degrees (Fig. 5). Only in the case of Na_2O vs Cl (Foresta Martin et al., 2019, 2020) are the confidence ellipses completely non-overlapping. The quantitative data of overlaps, inliers and outliers for each of the seven diagrams are provided in Table 5.

All seven provenance criteria examined identify some outliers that, compared to the number of inliers of each group, range between 2%-4%. The DPI (Discriminant Power Index), which jointly evaluates the percentage of overlapping confidence areas plus the percentage of outliers, assigns the first three positions, in order, to the following diagrams: Na_2O vs Cl (96,66%), Cl vs CaO/FeO (94,43%), SiO_2 vs K_2O/Na_2O (93%).

KDE with the Mahalanobis distance criterion at a 97.5% confidence level allows a robust, reproducible, and visually interpretable identification of confidence ellipses for each obsidian source, inliers and outliers. The method performs well both for big and small sample groups and remains consistent across geological and archaeological subsets.

Table 5. Mean % of confidence ellipses overlap, Mean % of inliers, Mean % of outliers, and Discriminant Power Index (DPI) of each bivariate plot.

Plot	Mean % Overlap	Mean % Inliers	Mean % Outliers	DPI	References
Na_2O vs Cl	0.00	96.66	3.34	96.66	Foresta Martin et al., 2019, 2020, and this study
CaO/FeOtot vs Cl	2.78	97.22	2.78	94.43	Giaccio et al., 2017
SiO_2 vs K_2O/Na_2O	4.02	97.02	2.98	93	Francaviglia, 1984
Na_2O vs Al_2O_3	4.94	97.16	2.84	92.22	Le Bourdonnec et al., 2010
sigma vs tau	9.25	96.08	3.92	86.83	Francaviglia, 1999
SiO_2 vs CaO	6.09	97.77	2.23	91.69	Tykot, 2002
log (SiO_2/Al_2O_3) vs log (CaO/Al_2O_3)	14.67	96.67	3.33	82	Orange et al., 2017

5.1 The best performance of Na_2O vs Cl diagram

The absence of overlap between the Mahalanobis confidence ellipses in the Na_2O vs Cl space drastically reduces the risk that an obsidian fragment from one source might plot inside the field of another, thereby preventing false provenance attributions. For this reason, Na_2O vs Cl diagram was chosen as the primary discriminant domain for the *Obsidian Sieve*. Before implementing the Excel-based tool, the distribution of each source in this bivariate space was inspected in detail (Fig. 6), and conservative compositional windows were defined by enclosing the core inlier region of each group within a minimum-maximum rectangle (Table 5). These windows intentionally reduce edge-case

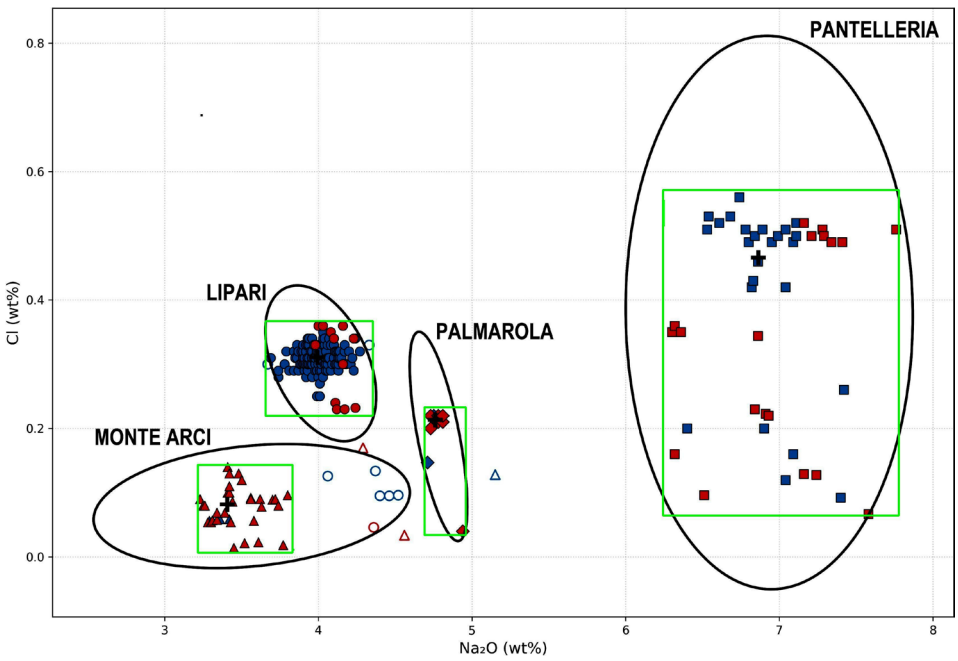

Figure 6. In the Na_2O vs Cl plane, the green rectangles restrict the fields of each source to the core of the inliers and define the minimum and maximum values of each coordinate. Legend as Fig. 5.

outliers, providing a highly conservative approach aimed at minimizing false positives. Let's take a detailed look at how data are distributed for each obsidian source in the Na_2O vs Cl space (Fig. 6; Table 5).

Monte Arci (Sardinia) sources are represented by 37 samples (32 geological and 5 archaeological). Despite its well-documented internal variability involving subsources SA, SB1, SB2, and SC (Tykot, 2002), in this study Monte Arci is treated as a single group. In the Na_2O vs Cl plot, the samples form a compact cluster with the lowest Na_2O (3.2-3.8 wt%) and Cl (0.01-0.14 wt%) values in the entire dataset. The KDE + Mahalanobis confidence ellipse at 97.5% confidence encloses 34 of the 37 entries, defining a stable and well-constrained inlier core that is clearly separated from Palmarola, Lipari, and Pantelleria. The three samples statistically indicated as outliers come from the Francaviglia papers. Two of them (Table 4/a, row 26, from Francaviglia, 1999; and row 31, from Francaviglia, 1984) are geological samples which exhibit slightly higher Na_2O contents (4.56 and 4.29 wt% respectively), falling just outside the edge of the confidence ellipse. Both are compatible with (i) limited secondary alteration and/or (ii) small-scale geochemical heterogeneity among the Monte Arci subdomains. The third outlier (Table 4/a, row 36, from Francaviglia, 1984) is an archaeological sample with an unusual high level of Na_2O (5.15 wt%), and likely it is a very altered sample.

Palmarola (Pontine Islands) sources exhibit fully compact behavior: all nine entries fall within the 97.5% confidence ellipse with no outliers. The Na_2O vs Cl window is small and internally consistent, reflecting the limited geological variability of the outcrop. The Na_2O range is very narrow (4.71-4.94 wt%); Cl range is much wide (0.04-0.22 wt%) giving the confidence ellipse a high eccentricity.

Pantelleria (Sicily Channel) sources show the highest Na_2O contents among Mediterranean obsidians (6.30-7.76 wt%), together with the highest Cl values (up to 0.56 wt%), both consistent with the peralkaline and volatile-rich nature of its magmatic system (Avanzinelli et al., 2004; Rotolo et al., 2020; Jordan et al., 2021). The KDE density surface is bimodal, reflecting two compositional sub-clusters corresponding to the northern (Lago di Venere-Fossa della Pernice) and southern (Balata dei Turchi-Salto La Vecchia) sectors of the pantelleritic system (Rotolo et al., 2020; Foresta Martin et al., 2020). Nevertheless, all 45 entries fall within the 97.5% ellipse, without outliers.

Lipari (Aeolian Islands) sources are the largest group, comprising 171 samples. Of these, 163 plot as inliers, while 8 lie outside the confidence ellipse. Two entries sit exactly on the 97.5% boundary (Table 4/d, rows 222 and 250, respectively from Foresta Martin et al., 2017, and Kasztovszky et al., 2019). These represent edge-case inliers that reflect the natural spread of the Lipari distribution. The remaining six outliers (Table 4, rows 251-256, five from Francaviglia and Piperno, 1987, and one from Francaviglia, 1999) show unusually low Cl values at otherwise typical Na_2O levels. These deviations may reflect analytical underestimation of Cl or selective volatile loss in altered samples.

Table 6. For each source: number of data, inliers, and outliers; ranges of sodium and chlorine in Na_2O vs Cl plot.

Source	N total	N inliers	N outliers	Na_2O min	Na_2O max	Cl min	Cl max
Monte Arci	37	34	3	3.23	3.8	0.014	0.14
Palmarola	9	9	0	4.71	4.94	0.04	0.22
Pantelleria	45	45	0	6.3	7.76	0.07	0.56
Lipari	171	162	9	3.69	4.27	0.23	0.36

6. The *Obsidian Sieve* working method

The methodology developed in this study culminates in the construction of the *Obsidian Sieve*, an Excel-based classification tool designed to provide a first-step provenance assessment of archaeological obsidians from the Central Mediterranean using only major and minor elements. The *Sieve* operates on the large geochemical dataset

assembled in this work and on the demonstrated discriminant power of the Na_2O vs Cl covariation space, which reliably separates the four Italian sources exploited in antiquity: Monte Arci, Palmarola, Pantelleria, and Lipari, as shown in previous studies (Foresta Martin et al., 2019, 2020).

The definition of source fields is based on the combined KDE + Mahalanobis statistical approach applied to Na_2O and Cl values. KDE (Kernel Density Estimation) is used to reconstruct the empirical probability distribution of each source, while Mahalanobis distance, computed at the 97.5% confidence level, defines robust confidence ellipses that separate inliers from outliers in a reproducible manner. The resulting ellipses are well defined for all four sources and show no overlap in the Na_2O vs Cl plane, confirming that this bivariate domain is the most effective discriminant space among all diagrams evaluated in this study.

The Excel file (.xls), provided as supplementary material, contains three operational worksheets. (i) The Database sheet includes the full set of geological and archaeological data for the four sources, expressed in wt% of major and minor oxides, along with their provenance designations as reported in the literature. (ii) The Sources sheet lists the four geological sources and the Unknown category, together with the minimum and maximum Na_2O and Cl values defining a conservative rectangular window around the statistical core of each source. These windows are intentionally narrow to exclude edge-case outliers and reduce the risk of false attributions. (iii) Finally, the Input sheet serves as the operational interface: the user pastes the analytical data of an archaeological specimen, and the tool automatically extracts Na_2O and Cl, compares them with the source windows, and returns the most probable provenance or, if no window is matched, the classification *Unknown*.

The internal logic of the tool follows a sequential series of checks, proceeding from Monte Arci to Palmarola, from Palmarola to Pantelleria, and finally to Lipari. At each step, the Na_2O-Cl pair is tested against the corresponding source window: if the values match, the attribution is immediate; if no window is satisfied, the fragment is assigned to the *Unknown* category. In practice, after the user inputs major/minor elements (including Na_2O and Cl) into the *Input* sheet, Na_2O and Cl values are extracted from the corresponding columns and the *Sieve* applies four sequential tests:

a. Do Na_2O and Cl fall within Monte Arci rectangle?
→ Yes → M.ARCI
→ No → go to next

b. Within Palmarola rectangle?
→ Yes → PALMAROLA
→ No → next

c. Within Pantelleria rectangle?
→ Yes → PANTELLERIA
→ No → next

d. Within Lipari rectangle?
→ Yes → LIPARI

e. If none of the four tests is satisfied → output = UNKNOWN

This selective procedure, implemented in the Excel spreadsheet (provided as Supplementary Material), is operationalised through nested IF and AND functions that retrieve the Na_2O and Cl threshold values directly from the "Sources" worksheet. The classification formula automatically compares the input Na_2O-Cl pair with the reference compositional windows defined for each source and returns the corresponding attribution or, if no window is satisfied, the output *Unknown*.

According to the rationale adopted here, *Unknown* specimens are those whose compositions may reflect hydration effects, alteration, analytical inaccuracies, or as-yet-unrecognized variability within known sources. They may also represent obsidians from sources outside the Central Mediterranean. In this sense, the *Unknown* category also acts as a safeguard against inadvertent misclassification of extra-regional obsidians within a Central Mediterranean framework. These specimens therefore constitute the best candidates for follow-up analyses using more sensitive instrumental techniques (high-precision XRF, LA-ICP-MS, or radiogenic isotopes), thus helping to optimise analytical time and cost.

The strength of the *Obsidian Sieve* lies in the convergence of three components: a broad database, a statistically robust and reproducible identification of source cores, and a simple operational implementation that can be used even

with low-cost analytical data (SEM-EDS, EMPA, XRF). While the compiled dataset inevitably reflects heterogeneous analytical protocols, it captures the main compositional trends of the four Italian obsidian sources as consistently reported in the literature, which is sufficient for the comparative and exploratory aims of this study. Owing to the conservative design of the source windows, the tool provides a cautious yet reliable first-level attribution that is fully consistent with the statistical model and with current geochemical knowledge of Central Mediterranean obsidians.

7. Results – Performance of the *Obsidian Sieve*

The combined KDE + Mahalanobis analysis carried out on the seven bivariate diagrams provides a quantitative basis for evaluating their relative discriminant performance. The metrics summarised in Table 5 – Mean % Overlap, Mean % Inliers, Mean % Outliers, and the Discriminant Power Index (DPI) – show that only one covariation space, Na_2O vs Cl, achieves complete separation among the four Central Mediterranean obsidian sources. This diagram exhibits the highest DPI value (96.66), negligible overlap among confidence ellipses, and a consistently low percentage of outliers across all sources. Two other systems, CaO/FeO_{tot} vs Cl and SiO_2 vs K_2O/Na_2O show moderately high scores but still display areas of inter-source superposition that make them unsuitable for unambiguous provenance assessment.

When examined in detail, the Na_2O vs Cl diagram reveals well-defined clusters for Monte Arci, Palmarola, Pantelleria, and Lipari. The KDE + Mahalanobis confidence ellipses at the 97.5% confidence level contain the substantial majority of samples for each source, with outliers representing only 2-4% of the dataset. The distribution of Pantelleria displays a characteristic bimodality associated with its northern and southern volcanic sectors, yet both clusters fall entirely within the same confidence ellipse. Lipari shows the largest number of edge-case specimens, including a group of low-Cl outliers already noted in the literature, but these do not compromise the overall separation among the four sources.

Based on these statistical results, conservative rectangular windows were defined for each source, enclosing their inlier cores within the Na_2O vs Cl space. These windows constitute the operational thresholds implemented in the *Obsidian Sieve*. Applied to the full dataset of 262 samples, the Sieve correctly assigns the vast majority of inliers to their respective geological sources, while the intentionally narrow limits result in a small proportion of specimens classified as *Unknown*. These unknown cases correspond primarily to statistical outliers, altered glasses with anomalously low Cl, or samples situated near the margins of the source clusters.

Overall, the performance of the *Obsidian Sieve* reflects its conservative design: it provides high-specificity source attribution for samples that fall within the well-defined Na_2O vs Cl windows, while effectively flagging ambiguous specimens for further investigation through higher-precision geochemical or isotopic methods. In this way, the Sieve functions as a reliable first-level screening tool, supporting efficient, cost-effective provenance analysis and guiding analytical effort toward the most problematic cases.

When the rectangular Na_2O vs Cl windows are applied to the full dataset of 262 samples, the *Obsidian Sieve* produces a small but informative fraction of *Unknown* classifications. These cases correspond closely to the statistical outliers identified through KDE + Mahalanobis analysis. Monte Arci shows three such specimens – two with marginally elevated Cl and one with slightly depressed Na_2O, while Lipari produces six *Unknowns,* all characterised by anomalously low Cl values already noted in previous studies. Pantelleria and Palmarola, by contrast, yield no *Unknowns*, reflecting both the compactness of their statistical cores and the robustness of the corresponding Na_2O vs Cl windows. We note that the robustness of statistical descriptors is inevitably reduced for sources represented by small sample sizes, such as Palmarola. This limitation further supports the conservative design of the *Obsidian Sieve*, including the explicit assignment of atypical samples to the *Unknown* category.

Overall, the proportion of *Unknown* cases corresponds to approximately 3-4% of the entire dataset, in line with the outlier percentages reported for each source. This behavior demonstrates that the Sieve's conservative design functions as intended: false-positive assignments are minimised, while samples exhibiting alteration, analytical deviation, or atypical Na_2O and Cl ratios are effectively isolated. These *Unknown* specimens therefore represent precisely the subset of artifacts that should be prioritised for follow-up investigation using high-precision geochemical or isotopic methods.

The complete methodological pathway leading to the development and application of the *Obsidian Sieve* is summarized in Fig. 7.

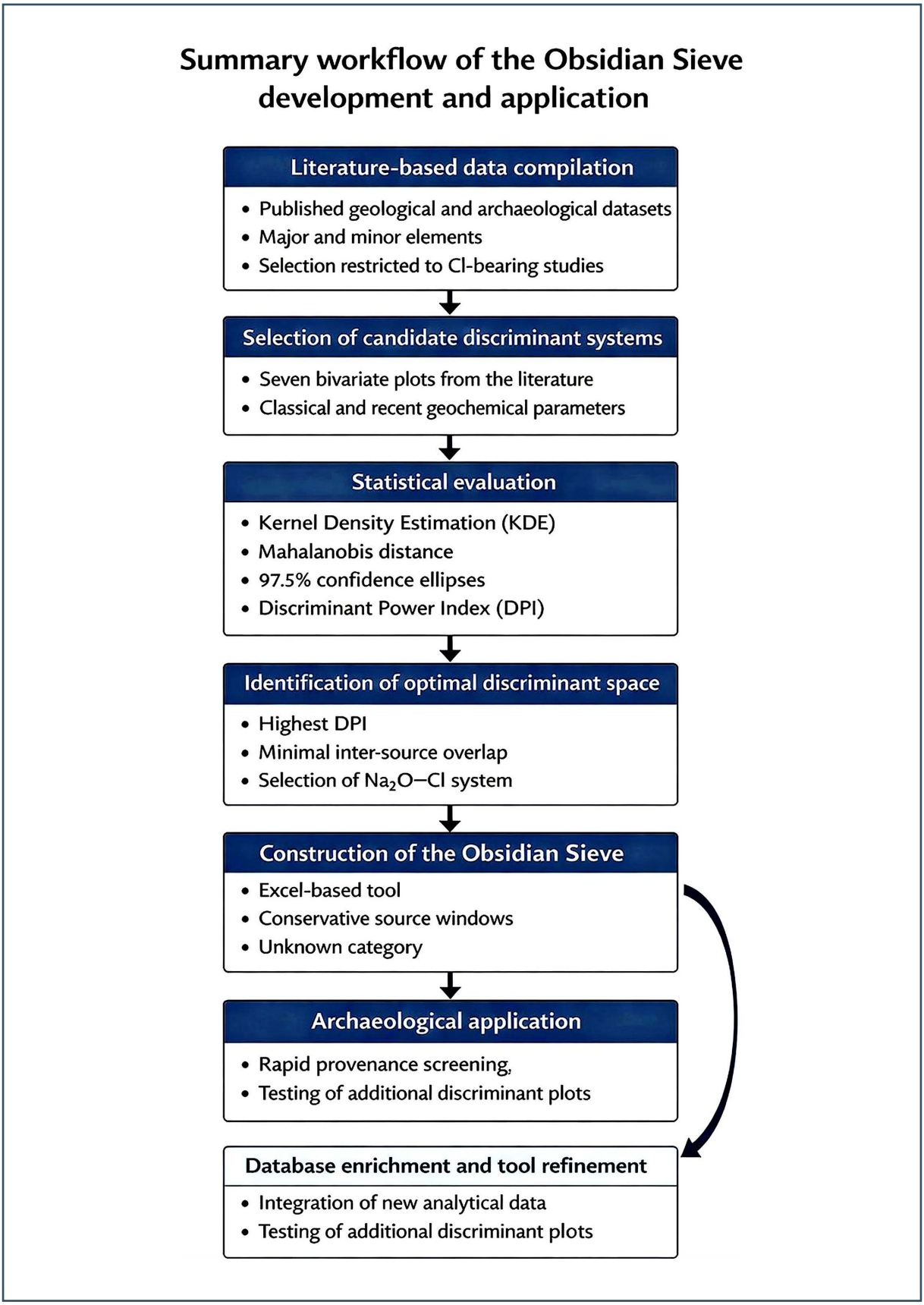

Figure 7. Summary workflow of the *Obsidian Sieve* development and application. Conceptual diagram illustrating the sequence of analytical and interpretative steps leading from literature-based data compilation to the construction and archaeological application of the *Obsidian Sieve*, including comparative evaluation of candidate discriminant systems, statistical validation, and iterative database enrichment.

8. Conclusion

Since the first systematic studies on obsidian provenance began in the second half of the last century, some of the most prolific researchers in this field have emphasized that a simple universal method for unequivocal diagnoses of the geological sources of obsidian artifacts does not exist (e.g., Francaviglia, 1984, 1999; Le Bourdonnec et al., 2010; Orange et al., 2017). We agree with this statement. Especially when the number of finds to be analyzed is large and includes mixed altered samples, provenance diagnosis can become complex and problematic, requiring time-consuming and expensive analytical procedures.

It is also evident that in the case of archaeological obsidian finds scattered across the vast Central-Western Mediterranean area, the original outcrops exploited in antiquity are limited to four sources well-known from a geological and geochemical perspective: Monte Arci, Palmarola, Pantelleria and Lipari. In most cases, it is possible to trace the artifacts to these sources simply by analyzing the major and minor elements through rapid and low-cost analyses.

The *Obsidian Sieve* we have proposed with this study, in the form of an Excel-based spreadsheet downloadable in the supplementary materials, offers the ability to input the results of major and minor element analyses – including the two highly discriminating parameters Na_2O and Cl – to obtain a rapid diagnosis of the geological sources of provenance, or of any problematic cases (*Unknown*) requiring further investigation.

Furthermore, the *Obsidian Sieve* is a flexible tool that can be enhanced by its users. It currently operates from a database of over 260 entries drawn from the literature. However, the user can expand the archive at will, making the *Obsidian Sieve* more effective in its selective and diagnostic capabilities. The validity of this tool could be extended also to other sources outside the Central Mediterranean area by adding suitable and updated datasets including Cl measurements, currently not available in the literature.

All things considered, in the era of machine learning applied to archaeometric studies, the *Obsidian Sieve* presents itself as a simple, streamlined tool, suitable for a preliminary and rapid obsidian provenance attribution.

The Excel file implementing the Obsidian Sieve is available as Supplementary Material and can be downloaded together with this article from the Annals of Geophysics website.

Acknowledgements. The author gratefully acknowledges the Italian Association of Volcanology (AIV) for organizing, on a biennial basis, a conference in memory of the volcanologist Alfred Rittmann, which includes a dedicated session fostering interdisciplinary dialogue among scholars in Earth Sciences, Geochemistry, Archaeology, and Cultural Heritage. The present study was developed within the framework of these interdisciplinary exchanges among researchers from scientific, historical, and humanistic disciplines.
Sincere thanks are also extended to the Editor and Editorial Board of *Annals of Geophysics* for organizing this special issue based on the contributions presented at the Rittmann 2024 Conference.
Finally, the author expresses deep appreciation to the three anonymous reviewers for their careful evaluation of this manuscript and for their valuable suggestions, which significantly contributed to improving both its content and presentation.

References

Acquafredda, P., T. Andriani, S. Lorenzoni and E. Zanettin (1999). Chemical characterization of obsidians from different Mediterranean sources by non-destructive SEM-EDS analytical method, J. Archaeol. Sci., 26, 3, 315-325, doi:10.1006/jasc.1998.0372.

Avanzinelli, R., L. Bindi, S. Menchetti and S. Conticelli (2004). Crystallisation and genesis of peralkaline magmas from Pantelleria Volcano, Italy: an integrated petrological and crystal-chemical study, Lithos, 73, 1-2, 41-69, doi:10.1016/S0024-4937(03)00081-1.

Barca, D., A. M. De Francesco and G. M. Crisci (2007). Application of Laser Ablation ICP-MS for characterization of obsidian fragments from peri-Tyrrhenian area, J. Cult. Herit., 8, 2, 141-150, doi:10.1016/j.culher.2006.12.001.

Barca, D., A. M. De Francesco, G. M. Crisci and C. Tozzi (2008). Provenance of obsidian artifacts from site of Colle Cera, Italy, by LA-ICP-MS method, Period. Mineral., 77, 41-52.

Baxter, M. J. (2003). Statistics in Archaeology, Arnold, London.
Bonifacie, M., N. Jendrzejewski, P. Agrinier, E. Humler et al. (2008). The chlorine isotope composition of Earth's mantle, Science, 319, 5869, 1518-1520, doi:10.1126/science.1150988.
Bowman, A. W. and A. Azzalini (1997). Applied Smoothing Techniques for Data Analysis, Oxford Univ. Press, Oxford.
Cann, J. R. and C. Renfrew (1964). The characterization of obsidian and its application to the Mediterranean region, Proc. Prehist. Soc., 30, 111-133, doi:10.1017/S0079497X00015097.
Cariddi, B., F. Foresta Martin, I. Arienzo, L. Giacomelli et al. (2026). Discriminating the origin of obsidian fragments in archaeological contexts based on morphological features and geochemical data: the Breccia Museo (Campanian Ignimbrite eruption, Italy) case study, Ann. Geophys., 69, doi:10.4401/ag-9428.
Carroll, M. R. (2005). Chlorine solubility in evolved alkaline magmas, Ann. Geophys., 48, 4-5, doi:10.4401/ag-3223.
Carroll, M. R. and J. D. Webster (1994). Solubilities of sulfur, noble gases, nitrogen, chlorine, and fluorine in magmas, Rev. Mineral. Geochem., 30, 1, 231-279, doi:10.1515/9781501509674-013.
Carter, T. (2014). The consumption of obsidian in the Early Bronze Age Aegean, in Networks of Trade and Exchange in the Aegean Bronze Age C. Knappett (Ed.), Routledge, London, 59-83.
De Francesco, A. M., G. M. Crisci and M. Bocci (2008). Non-destructive analytic method using XRF for determination of provenance of archaeological obsidians from the Mediterranean area: a comparison with traditional XRF methods, Archaeometry, 50, 2, 337-350, doi:10.1111/j.1475-4754.2007.00355.x.
Forenbaher, S. (2018). Special Place, Interesting Times: The Island of Palagruža and Transitional Periods in Adriatic Prehistory, Archaeopress, Oxford.
Foresta Martin, F., A. Di Piazza, C. D'Orìano, M. L. Carapezza et al. (2017). New insights into the provenance of the obsidian fragments of the island of Ustica (Palermo, Sicily), Archaeometry, 59, 3, 435-454.
Foresta Martin, F., S. G. Rotolo, M. Nazzari and M. L. Carapezza (2019). Chlorine as a discriminant element to establish the provenance of Central Mediterranean obsidians, Poster presentation, International Workshop "The Black Gold That Came from the Sea", Palermo, Italy, June 2019.
Foresta Martin, F., S. G. Rotolo, M. Nazzari and M. L. Carapezza (2019). Chlorine as a discriminant element to establish the provenance of Central Mediterranean obsidians, Open Arch., 6, 1, 454-476.
Foresta Martin, F. (2024). L'Ossidiana: come un vetro vulcanico diventò l'oro nero della Preistoria, in L'oro nero del Mediterraneo, Villaggio Letterario, Napoli, 17-42, ISBN:979-12-80974-15-0.
Francaviglia, V. (1984). Obsidian characterization by chemical methods, Archaeometry, 26, 3, 315-322.
Francaviglia, V. M. and M. Piperno (1987). La répartition et la provenance de l'obsidienne archéologique de la Grotta dell'Uzzo et de Monte Cofano (Sicile), ArchéoSciences, 11, 1, 31-39.
Francaviglia, V. (1988). Ancient obsidian sources on Pantelleria (Italy), J. Archaeol. Sci., 15, 2, 109-122.
Francaviglia, V. (1999). Caratterizzazione chimica e provenienza delle ossidiane mediterranee, Rend. Lincei, 10, 3, 321-330.
Freund, K. P. (2018). A long-term perspective on the exploitation of Lipari obsidian in central Mediterranean prehistory. Quat. Int., 468, 109-120, doi:10.1016/j.quaint.2017.10.014.
Giaccio, B., E. M. Niespolo, A. Pereira, S. Nomade et al. (2017). First integrated tephrochronological record for the last ~190 kyr from the Fucino Quaternary lacustrine succession, central Italy, Quat. Sci. Rev., 158, 211-234, doi:10.1016/j.quascirev.2017.01.004.
Gottini, J. (1968). An empirical classification of Italian volcanic rocks based on alkaline variations, Bull. Volcanol., 31, 4, 313-319.
Hyndman, R. J. (1996). The problem with boundary bias in kernel density estimation, Aust. J. Stat., 38, 3, 199-210.
Jordan, N. J., J. C. White, R. Macdonald and S. G. Rotolo (2021). Evolution of the magma system of Pantelleria (Italy) from 190 ka to present, C. R. Geosci., 353, S2, 133-149, doi:10.5802/crgeos.61.
Kasztovszky, Z., K. T. Biró, I. Nagy-Korodi, S. J. Sztáncsuj et al. (2019). Provenance study on prehistoric obsidian objects found in Romania using prompt gamma activation analysis, Quat. Int., 510, 76-87, doi:10.1016/j.quaint.2018.11.024.
Le Bas, M. J. (1986). A chemical classification of volcanic rocks based on the total alkali-silica system, J. Petrol., 27, 247-257.
Le Bourdonnec, F., X. Bontempi, J. M. Marini, N. Mazet et al. (2010). SEM-EDS characterization of western Mediterranean obsidians and the Neolithic site of A Fuata (Corsica), J. Archaeol. Sci., 37, 92-106.
Lowenstern, J. B. (1994). Chlorine, fluid immiscibility, and degassing in peralkaline magmas from Pantelleria, Italy, Am. Mineral., 79, 3-4, 353-369.

Macdonald, R. and R. L. Smith (1992). Chemistry of the subalkalic silicic obsidians, U.S. Gov. Print. Off., Washington.
Mahalanobis, P. C. (1936). On the generalized distance in statistics, Proc. Natl. Inst. Sci. India, 2, 49-55.
Métrich, N. and M. J. Rutherford (1992). Experimental study of chlorine behavior in hydrous silicic melts, Geochim. Cosmochim. Acta, 56, 2, 607-616, doi:10.1016/0016-7037(92)90108-D.
Orange, M., F. X. Le Bourdonnec, L. Bellot-Gurlet, C. Lugliè et al. (2017). On sourcing obsidian assemblages from the Mediterranean area: analytical strategies for their exhaustive geochemical characterization, J. Archaeol. Sci. Rep., 12, 834-844, doi:10.1016/j.jasrep.2016.12.021.
Peacock, M. A. (1931). Classification of igneous rock series, J. Geol., 39, 1, 54-67.
Rittmann, A. (1957). Die Struktur der magmatischen Gesteine als Teil der allgemeinen Struktur der Lithosphäre, Schweiz. Mineral. Petrogr. Mitt., 37, 79-102.
Rittmann, A. (1962). Vulkane und ihre Tätigkeit (2nd ed.), Schweizerbart, Stuttgart.
Rittmann, A. (1973). Chemical characteristics of basic and ultrabasic rocks and some general comparisons with intermediate and acid rocks, Bull. Volcanol., 37, 2, 596-609.
Rollinson, H. R. and V. Pease (2021). Using Geochemical Data: To Understand Geological Processes, 2nd ed., Cambridge Univ. Press, Cambridge, doi:10.1017/9781108777834.
Rotolo, S. G., M. L. Carapezza, A. Correale, F. Foresta Martin et al. (2020). Obsidians of Pantelleria (Strait of Sicily): a petrographic, geochemical and magnetic study of known and new geological sources, Open Archaeol., 6, 1, 434-453, doi:10.1515/opar-2020-0120.
Ruka, R., M. L. Galaty, D. J. Riebe, R. H. Tykot et al. (2019). PXRF analysis of obsidian artifacts from Albania: crossroads or cul-de-sac?, J. Archaeol. Sci. Rep., 24, 39-49, doi:10.1016/j.jasrep.2018.12.014.
Scott, D. W. (1979). On optimal and data-based histograms, Biometrika, 66, 605-610.
Scott, D. W. (2015). Multivariate Density Estimation: Theory, Practice, and Visualization, Wiley, Hoboken.
Shand, S. J. (1927). Eruptive rocks: their genesis, composition, classification, and their relation to ore-deposits, with a chapter on meteorites, Murby, London.
Silverman, B. W. (1986). Density Estimation for Statistics and Data Analysis, Chapman and Hall, London.
Tykot, R. H. (1996). Obsidian procurement and distribution in the central and western Mediterranean, J. Mediterr. Archaeol., 9, 1, 39-82, doi:10.1558/jmea.v9i1.39.
Tykot, R. H. (2002). Chemical fingerprinting and source tracing of obsidian: the central Mediterranean trade in black gold, Acc. Chem. Res., 35, 8, 618-627, doi:10.1021/ar000208p.
Tykot, R. H. (2017). Obsidian studies in the central Mediterranean: 25 years of research, Open Archaeol., 3, 1, 264-278, doi:10.1515/opar-2017-0019.
Tykot, R. H. (2019). Geological sources of obsidian on Lipari and artifact production and distribution in the Neolithic and Bronze Age central Mediterranean, Open Archaeol., 5, 83-105, doi:10.1515/opar-2019-0007.
Tykot, R. H. (2021). Non-destructive pXRF analysis of prehistoric obsidian artifacts from the central Mediterranean, Appl. Sci., 11, 16, 7459, doi:10.3390/app11167459.
Williams-Thorpe, O., S. E. Warren and J. G. Nandris (1984). The distribution and provenance of archaeological obsidian in Central and Eastern Europe, J. Archaeol. Sci., 11, 3, 183-212.
Williams-Thorpe, O. (1995). Obsidian in the Mediterranean and the Near East: a provenancing success story, Archaeometry, 37, 2, 217-248, doi:10.1111/j.1475-4754.1995.tb00738.x.

***CORRESPONDING AUTHOR: Franco FORESTA MARTIN**,
Istituto Nazionale di Geofisica e Vulcanologia, Sezione di Palermo, Italy
e-mail: franco.forestamartin@ingv.it